A dish–stirling solar concentrator coupled to a seasonal thermal energy storage system in the southern mediterranean basin: A cogenerative layout hypothesis

Article *in* Energy Conversion and Management · October 2020

DOI: 10.1016/j.enconman.2020.113228

CITATIONS
10

READS
234

5 authors, including:

Stefania Guarino
Università degli Studi di Palermo
8 PUBLICATIONS **48** CITATIONS
SEE PROFILE

Alessandro Buscemi
Università degli Studi di Palermo
15 PUBLICATIONS **60** CITATIONS
SEE PROFILE

Ciulla Giuseppina
Università degli Studi di Palermo
77 PUBLICATIONS **2,444** CITATIONS
SEE PROFILE

Marina Bonomolo
Università degli Studi di Palermo
53 PUBLICATIONS **687** CITATIONS
SEE PROFILE

Please cite this paper as:

Guarino, S., Buscemi, A., Ciulla, G., Bonomolo, M., & Brano, V. L. (2020). A dish-stirling solar concentrator coupled to a seasonal thermal energy storage system in the southern mediterranean basin: A cogenerative layout hypothesis. Energy Conversion and Management, 222, 113228.

https://doi.org/10.1016/j.enconman.2020.113228

A dish-Stirling solar concentrator coupled to a seasonal thermal energy storage system in the Southern Mediterranean basin: a cogenerative layout hypothesis

Stefania Guarino[1,*], Alessandro Buscemi[1], Giuseppina Ciulla[1], Marina Bonomolo[1], Valerio Lo Brano[1]

[1]Department of Engineering
University of Palermo, Palermo, Italy
e–mail: stefania.guarino@unipa.it, alessandro.buscemi@unipa.it, giuseppina.ciulla@unipa.it, marina.bonomolo@unipa.it; valerio.lobrano@unipa.it

ABSTRACT

In the future, renewable energy sources will increasingly represent an efficient energy source capable of meeting the demands of residential and industrial buildings avoiding the emissions of greenhouse gases into the atmosphere. In this paper, a heat and electric power cogeneration plant implementing a field of dish-Stirling collectors, a seasonal geothermal storage and a system of water-to-water heat pumps is proposed for the first time. The cogeneration plant has been designed both to supply thermal energy to the heating system of Building 9 of the Department of Engineering in Palermo and to produce electricity. The operation of the plant has been tested by means of hourly-based numerical simulations that have been carried out using a numerical model implemented with Transient System Simulation Tool. The experimental data of a pilot dish-Stirling collector, located in the same area, has been used to carefully calibrate the numerical model. Using energy and economic performance indicators, it

* Corresponding author

was possible to select the best configurations among 1440 analysed cases. Results of simulations show that with the best plant configuration, it is possible to cover 97% of the building's annual thermal loads with energy produced by the solar system. The remaining 64% of electrical energy produced by the electric engines is free to be used for other applications. Financial analyses have shown that market penetration of this type of plant would need a strong support through incentives.

KEYWORDS

CSP technology, dish-Stirling concentrator, cogeneration, geothermal systems, thermal energy storage systems.

HIGHLIGHTS

- Layout for a dish-Stirling coupled to a geothermal storage system presented
- Energy performance of the cogenerative solar concentrator presented
- Influence of several physical parameters investigated to optimise the system
- Identification of a incentivisation policy for a cogenerative dish-Stirling plant
- Evaluation of energy and economic viability of the cogenerative layout

1. INTRODUCTION

Much research nowadays focuses on climate change due essentially to continuous, massive emissions of Greenhouse Gases (GHG) into the atmosphere. The increase in global average temperature and greenhouse gas concentrations continues to grow [1] and there is a strong correlation between fossil fuel energy production and climate change. The main human activities that give rise to CO_2 emissions are: energy production by transformation and combustion of fossil fuels, and energy use in industry, transport, and heating and cooling of buildings [2]. In particular, the energy needs of the building are essentially dependent on the performance of the employed heating system [3], on the building envelope characteristics, but also on the climatic conditions of the site where it is located [4]. Renewable sources, such as wind and solar, represent a valid alternative to fossil fuels [5], and would efficiently satisfy the energy demand of residential and industrial buildings, both saving energy and avoiding emissions into the atmosphere [6]. The major challenge for technologies that use renewable sources is that of matching the fluctuation of energy production to the energy demand [7]. In fact, compared to traditional power plants, the large variability in the end-user demands

(electricity, heating and cooling energy), coupled with the uncertainty in solar and wind energy availability, requires the adoption of energy storage systems for dampening the intermittency problems and for performing peak shaving [8]. In this framework, Concentrating Solar Power (CSP) is one of the most interesting and efficient technologies used to produce heat and electricity by Renewable Energy Sources (RES) [9]. There are four main CSP technologies: parabolic trough collector systems; linear Fresnel reflector systems; central receiver tower systems; and parabolic dish collector systems [12].

Among CSP systems, the parabolic dish concentrator is the most efficient technology in the conversion of solar energy into thermal energy [13]. Usually, parabolic dish collectors are coupled with a Stirling engine, an alternative, external combustion engine mounted on the focal point of the dish, in which the working fluid performs the homonymous cycle [14]. CSP systems have the best performance when installed in locations with high DNI levels [15], since direct sunlight is the main meteorological parameter that most affects the energy yield of such systems [16]. Dish-Stirling systems can be used in many applications [9], such as: in micro-cogeneration to generate heat and electricity simultaneously [17]; in integration with heating, ventilation and air conditioning technology to fulfil the heating, cooling, electricity and domestic hot water demands of a residential building [18]; in integration with thermal energy storage [19] or hybridisation using other RES [20]; in standalone power generation to bring electricity to remote rural areas [21]; in centralised power generation [22]; and in potable water production [23] and water pumping [24].

The exploitation of waste low-temperature heat from a Stirling engine that could be used to cover the winter heating load of buildings [18]. It is, however, necessary to resolve the usual mismatch between the thermal energy production (summer) and the thermal energy demand periods (winter) through a Seasonal Thermal Energy Storage system (STES) [25]. In this framework, geothermal plants can be considered a promising residential heating source due to its high efficiency [26] for example installing a solar-assisted ground source heat pump as described in [27] and [28]. There are different types of STES systems [29], such as: Hot Water Thermal Energy Storage (HWTES); Gravel-Water thermal energy storage (GWTES); Aquifer Thermal Energy Storage (ATES); and Borehole Thermal Energy Storage (BTES).

HWTES systems store hot water inside a tank with a reinforced concrete structure which can be buried in the ground. The tank is provided with thermal insulation in order to minimise heat losses to the environment [29]. Similarly, GWTES systems store heat inside a reinforced concrete and thermally insulated tank, but contain a mixture of water and gravel [29]. This

mixture is characterised by a lower specific heat compared to water and, therefore, considering the same thermal energy storage, GWTES systems are larger than HWTES systems [30]. ATES systems are an interesting alternative because it is not necessary to build a reinforced concrete tank nor to excavate a site in which to bury it as ATES heat storage exploits already existing aquifers in the subsoil [30]. Finally, BTES systems use soil as the storage medium. In this case, the heat is transferred to the soil by a system of distributed vertical geothermal exchangers [31]. The heat transfer fluid, usually a solution of water and glycol, flows along the borehole exchanger charging and discharging the soil creating a radial temperature gradient that reduces the external heat losses to the undisturbed cooler soil surrounding the storage volume. The BTES system can also be thermally insulated on the upper boundary surface in order to limit the influence of external climate conditions and to minimise the upper thermal losses [32].

Among the aforementioned sensible thermal energy storage systems, BTES systems are the most suited to be coupled with dish-Stirling CSP technology because of: the low operating temperature, the relative ease of installation, the moderate investment needed to realise the geothermal field [33], and the medium-high value of storage yield [29], since thermal energy losses in the environment are limited as a result of the low enthalpy that characterises the storage process and therefore the low temperature of the heat transfer fluid used. BTES plants are already widely used worldwide [34]. In Sweden, several single-U boreholes have been installed in a parking lot and have been used for both summer and winter air conditioning in a university building since 2001 [35].

At present, to the authors' knowledge, it is possible to find in the literature studies on the use of a dish-Stirling system in a cogeneration setup [36], but there are no studies in particular investigating the possibility of coupling the dish-Stirling solar concentrator to the seasonal boreholes storage system. Examining the dish-Stirling system currently installed on the University campus of Palermo and Building 9 of the Engineering Department next to the site where the same production system is located, this article proposes a layout of the Combined Heat and Power (CHP) plant in order to meet the space heating load of Building 9 through the low-temperature waste heat from the Stirling engine. The proposed plant layout includes: a number of dish-Stirling units for the production of electricity and heat; a BTES-type seasonal thermal storage system with a number of possible geometries; two heat pumps; and a thermal user consisting of Building 9 where the natural gas boiler is kept as an auxiliary system.

According to the research exposed in this work, the proposed cogeneration plant layout would completely satisfy the thermal energy needs of the building considered, obtaining significant

energy savings and large amounts of avoided CO_2 emissions. However, the economic feasibility of these systems is strongly correlated to the ability to optimise the plant configuration so that the proceeds of energy sales and the energy savings, obtained over the operating life of the plant, can balance the total cost of installation. For this reason, an incentivisation scheme is proposed in order to encourage commercial penetration in the residential sector of the examined CHP system.

2. DESCRIPTION OF PROPOSED COGENERATIVE LAYOUT AND ITS OPERATION

The proposed system is essentially a combination of a Concentrating Solar Power (CSP) and a Borehole Thermal Energy Storage (BTES) system. The CSP plant produces electricity mainly during the summer period. The waste heat produced during the operation of the CSP system is used to heat a volume of soil through a system of geothermal heat exchangers. The thermal energy stored during the summer period is partially recovered from the soil during the winter period, and is used as a cold heat source for the heat pump system providing the heating of the building.

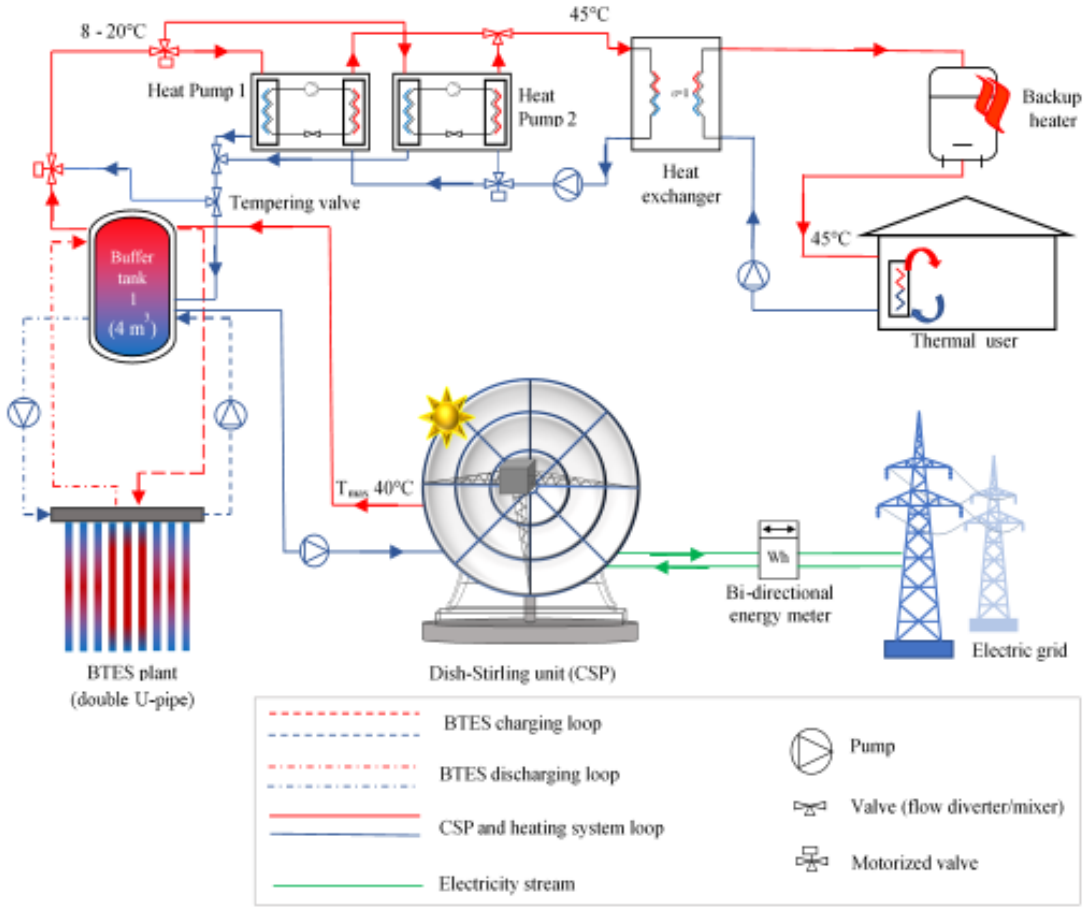

Figure 1: Schematic representation of the proposed CHP plant.

Figure 1 shows the layout of the proposed system with its different components:

- A CSP collector system consists of dish-Stirling units. Each unit is characterised by a rated electrical output power of about 30 kWe (corresponding to a rated DNI of about 960 W/m^2 [37]. The electric generators of the units are connected to the electric grid through a bi-directional energy meter, while the closed cooling circuits of the Stirling engines are connected to a Short-Term Thermal Energy Storage (STTES).
- A BTES system consists of a system of vertical ground-coupled heat exchangers with a double-U configuration, spatially distributed in the soil volume along concentric rings. The terminals of the closed circuit of the BTES exchanger pipes are connected to the STTES.
- Two water-to-water heat pumps are connected in parallel (with nominal heating capacities of 200 kW$_{th}$ and 300 kW$_{th}$ respectively). The cold side of this system is connected to the STTES while the hot side transfers heat to the heating system of the building through a thermal heat exchanger.

- An STTES (with a volume of about 4 m^3) acts as a hydraulic disconnector between the closed circuits of the Stirling engine's cooling system, the BTES, and the hot sides of the thermal exchangers of the heat pump evaporators.
- The closed circuit of the building's heating system is realised by connecting a heat exchanger to the condensers of the heat pumps, a conventional (gas-fired) backup boiler and hydronic terminals made with a system of fan coils.

The central element of the proposed plant is the system of dish-Stirling solar collectors generating the electricity that is injected into the national grid. The bidirectional meter is necessary because the CSP collectors during their operation, also consume a small amount of energy for the electrical parasitic absorption related to the operations of both the sun tracking system and the circulation pumps of the Stirling engine cooling system. The net electrical power produced by the dish-Stirling plant is usually linearly correlated to the value of DNI, as shown in the literature for this type of system [37]. On the other hand, data measured during an experimental campaign on the operation of the CSP model chosen for this study [37] has shown that the outlet temperature of the fluid in the cooling circuit of the Stirling engine is always around 40 °C independent of solar irradiation levels. This low-temperature thermal energy source in the studied layout is injected into the BTES, through the STTES mainly in the summer period when there is the highest energy production from the collectors.

In the winter period, when there is a heating demand from the building, the thermal energy stored in the BTES is transferred to the evaporators of the heat pumps. When the heating demand is simultaneous with the operations of the CSP system (e.g. on a cold winter day with clear skies), the thermal energy from the cooling of the Stirling engines is directly transferred to the heat pumps through the STTES. The water-to-water heat pump system is set to heat the water circulating in the heating circuit (user side) to a fixed temperature of 45 °C by means of a heat exchanger. As depicted in Figure *2*, the BTES is essentially formed by a cylindrical portion of soil in which a number of vertical boreholes are drilled. In each borehole, a heat exchanger is installed, which is sealed by a grout mixture to guarantee the thermal contact between the soil and the pipes of the exchanger. In the configuration proposed by this study, the heat exchangers, realised with double-U pipes are arranged on concentric rings. The heat exchangers placed in the inner ring are connected to each other in parallel. Then, each of these exchangers is connected in series to another exchanger placed in the next outer ring which, in turn, is connected to another one located in the next outer ring and so on.

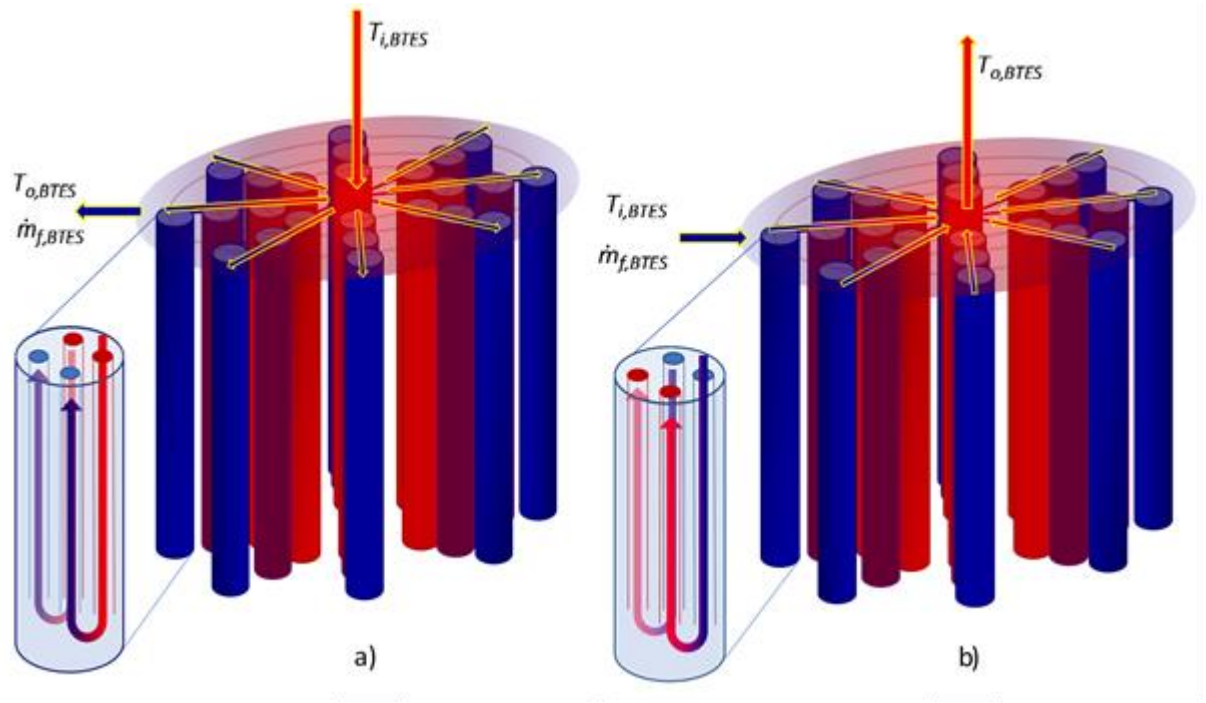

Figure 2: Operation of the BTES: a) charging phase (summer period) and b) discharging phase (winter period)

Finally, all the exchangers of the outermost ring are connected to each other in parallel. During this thermal charging, the hot fluid enters the central exchangers of the BTES and returns to the STTES from the more external ones (see Figure *2*a). Vice versa, during the thermal discharge stage (winter period), the cold fluid coming from the STTES enters from the outermost BTES boreholes and returns, heated, to the central ones (see Figure *2*b). In this way it is possible to generate, over time, a radial thermal gradient (thermocline) in the BTES soil volume: the highest soil temperatures are localised in its central part and the lowest in its periphery. The thermocline formation increases the storage efficiency and reduces the thermal losses between the BTES soil volume and the cold soil surrounding it.

Finally, technical sheets of the heat pumps used for this study indicate that they can operate with cold source temperatures at the evaporators ranging from 8 °C to 20 °C. Therefore, to avoid the evaporator of the heat pumps getting water at a temperature higher than that allowed by the technical specifications, a tempering valve allows the mixing of hot water coming from STTES with cold water coming back from the evaporators so as to guarantee a maximum delivery temperature of 20 °C. Finally, when the renewable energy production system fails to fully cover the building's thermal loads, a natural gas-powered backup boiler is switched on to ensure that the fan coils are always fully operational. In this study, it is shown, through parametric analyses conducted with a dynamic numerical model, how the different components

of the proposed CHP system can be optimised to minimise fossil fuel consumption, and, therefore, CO_2 emissions compared to a conventional heating system.

2.1 DISH-STIRLING SYSTEM MODEL

In order to simulate electrical and thermal energy production of each dish-Stirling collector of the CSP plant, reference was made to the numerical model elaborated and tested using the experimental operating data of the CSP plant in Palermo [37]. This model, which allows the calculation of the output of the plant as a function of DNI and air temperature variations, is based on a thermal balance of the system and on an experimental curve representing the mechanical efficiency at partial loads of the Stirling engine.

The direct radiation is reflected and concentrated on the focus of the parabolic collector where the receiver of the Power Conversion Unit (PCU) is located. The heat power effectively absorbed by the receiver can be calculated as:

$$\dot{Q}_{r,in} = I_b \cdot A_n \cdot \eta_o \cdot \eta_{cle} \tag{1}$$

where, I_b is the solar beam radiation, A_n is the net effective surface of mirrors, η_o is the optical efficiency of the collector with clean mirrors and η_{cle} is the cleanliness index of the mirrors (a parameter related to the soiling of the mirrors which ranges between 0 and 1).

However, part of the energy absorbed by the receiver is dispersed into the environment due to convective and radiative heat losses. These losses can be calculated, in a simplified way, using the following expression [37]:

$$\dot{Q}_{r,out} = A_r \cdot \left\{ h_r \cdot (T_r - T_{air}) + \sigma \cdot \varepsilon_r \cdot \left[(T_r + 273.15)^4 - (T_{sky} + 273.15)^4 \right] \right\} \tag{2}$$

where A_r is the receiver aperture area, h_r is the effective receiver convective coefficient, T_r and T_{air} are the receiver and the ambient temperatures respectively, σ is the Stefan-Boltzmann constant, ε_r is the effective emissivity of the receiver and T_{sky} is the apparent sky temperature. The empirical expression used for the estimation of sky temperature (expressed in degree Celsius) is the following:

$$T_{sky} = 0.0552 \cdot (T_{air} + 273.15)^{1.5} - 273.15 \tag{3}$$

where T_{air} is expressed in degree Celsius. Thus, by means of the energy balance of the receiver it is possible to calculate the thermal input power to the Stirling motor as the difference between the thermal power absorbed by the receiver and that dispersed from it:

$$\dot{Q}_{s,in} = \dot{Q}_{r,in} - \dot{Q}_{r,out} \tag{4}$$

From the balance of the Stirling engine, instead, it is possible to obtain the thermal power output of the engine by the following difference:

$$\dot{Q}_{S,out} = \dot{Q}_{S,in} - W_S \tag{5}$$

where W_S is the mechanical output power of the Stirling engine, which is itself a function of both the thermal input power and the ambient temperature.

Moreover, as shown in [37], based on the analysis of the operational data of numerous different real-functioning dish-Stirling units, it is possible to approximate the mechanical efficiency curve of the Stirling engine at partial loads as:

$$\eta_{S,M} = \left(a_1 - \frac{a_2}{\dot{Q}_{S,in}} \right) \cdot R_T \tag{6}$$

where a_1 and a_2 are two fitting constants and R_T is a correction factor which takes into account the effect of the variations of T_{air} on the efficiency of the engine:

$$R_T = \left(\frac{T_0 + 273.15}{T_{air} + 273.15} \right) \tag{7}$$

where T_0 is a fixed parameter representing the reference temperature. Thus, using Eq. 6, the mechanical output power of the engine can be expressed as:

$$W_S = (a_1 \cdot \dot{Q}_{S,in} - a_2) \cdot R_T \tag{8}$$

Finally, substituting Eq. 8 into Eq. 5 it is possible to obtain an expression of the thermal output power of the engine as a function of the thermal input power:

$$\dot{Q}_{S,out} = \dot{Q}_{S,in} \cdot \eta_{S,T} \tag{9}$$

where $\eta_{S,T}$ is the thermal efficiency of the Stirling engine that is related to the mechanical efficiency of the engine by the following expression:

$$\eta_{S,T} = 1 - \eta_{S,M} \tag{10}$$

Eq. 9 can be applied to calculate the power that needs to be dissipated by the Stirling engine to ensure its operation. In the CHP plant proposed by this study, this waste heat is used to thermally charge the BTES. To define the electrical producibility of the dish-Stirling collector, reference is made to the following equation that has been proposed in [37] for the purpose of

simulating the gross electrical power output from a dish-Stirling collector as a function of the direct normal irradiation, the air temperature and the mirror cleaning index:

$$E_g\left(I_b, T_{air}, \eta_{cle}\right) = \left(\eta_e \cdot \eta_o \cdot \eta_{cle} \cdot a_1 \cdot A_n \cdot R_T\right) \cdot I_b - \left\lfloor \eta_e \cdot \left(a_1 \cdot Q_{r,out} + a_2\right) \cdot R_T \right\rfloor \quad (11)$$

where η_e is the electric efficiency of the alternator. Finally, by subtracting from the gross electrical power the parasitic electrical absorption of the system (due to the operation of both the solar tracker and the circulation pumps of the Stirling engine cooling system), it is possible to calculate the net electrical output power of the system as:

$$E_n = E_g - E_p \quad (12)$$

The model parameters that were used for the simulations are summarised in Table 1. These are the parameters characteristic of the commercial version of the pilot plant currently operating at the University of Palermo [37]. In particular, as reported in the same table, an average value of the parasitic electric absorption E_p^{ave} and an average value of the mirror cleaning index η_{cle}^{ave} were fixed according to the specific experience gained from the analysis of the real operating data of this collector [37].

Table 1: Parameters defined for the dish-Stirling model.

Parameters	**Value**	**Units**
Effective aperture area A_n	106	m^2
Receiver aperture area A_r	0.0314	m^2
Clean mirrors optical efficiency η_o	0.85	-
Receiver convective coefficient h_r	10	$W/(m^2 \cdot K)$
Receiver effective emissivity ε_r	0.88	-
Parameter a_1 of Eq. 6	0.475	
Parameter a_2 of Eq. 6	3.319	kW
Reference temperature T_0	25	°C
Electrical efficiency of the *CPU*, η_e	0.924	-
Average parasitic absorption E_p^{ave}	1.60	kW
Average cleanliness index η_{cle}^{ave}	0.90	-

2.1.1 Evaluating accuracy of the dish-Stirling system model

The model for predicting the energy producibility of the dish-Stirling described above has been recently developed and presented in research work [37]. The model, which takes into account

the salient characteristics of the dish-Stirling plant and the climatic variables, has been calibrated and verified by comparing the predicted values with the actual measured values. In order to measure the quality and accuracy of the model, an error analysis was carried out. To this aim, the Mean Absolute Percentage Error (MAPE) is one of the most common indexes used to quantitatively assess the goodness of a model. MAPE allows the consideration of a set of calculated and measured couples of values and provides an average of the absolute relative error according to Eq. 13:

$$MAPE = \frac{100}{n} \cdot \sum_{i=1}^{n} \left| \frac{y_i - x_i}{x_i} \right| \tag{13}$$

where: n indicates the number of value pairs and y and x are, respectively, the predicted and measured value of the i-th pair considered [38]. This index is easy to calculate and is particularly intuitive but, nevertheless, recent studies show that this metric has some weak points: the value of this index loses meaning when the measured value is zero, and it also shows an asymmetric behaviour depending on whether the examined model tends to overestimate or underestimate. A new index has recently been proposed to solve these problems by introducing a robust, symmetric measure based on the natural log accuracy ratio [38].

The accuracy ratio (Q), that is the ratio between the predicted value (y) and the measured value (y), is defined by Eq. 14:

$$Q = \frac{y}{x} \tag{14}$$

The error measurement can be made using the median symmetric accuracy (ζ) defined by Eq. 15:

$$\zeta = 100 \cdot \left(\exp\left(M\left(\left| \log_e\left(Q \right) \right| \right) \right) - 1 \right) \tag{15}$$

where, M is the median function used to aggregate over all prediction-observation pairs.

To evaluate the accuracy of the model used, Authors employed about 2000 net power values generated by the dish-Stirling system in Palermo under clean mirror conditions. MAPE and median symmetric accuracy are both provided to allow easy comparison with other models. The values summarised in Table 2 attest to a more than good reliability of the proposed model.

Table 2: Accuracy of the dish-Stirling model

Metric of accuracy	Error [%]

MAPE	3.22
ζ	1.90

2.2 GEOTHERMAL ENERGY STORAGE SYSTEM MODEL

The Duct Ground Heat Storage Model (DST was used to simulate numerically the transient thermal response of the borehole system that constitute the BTES. This model, implemented in the Transient System Simulation Tool (TRNSYS) Type 557, can be used successfully to analyse the seasonal storage of thermal energy in the soil [34]. According to the DST, the boreholes of the plant are uniformly distributed in a volume of soil (arranged in a hexagonal pattern). The conventional volume of BTES defined by this system can be estimated as:

$$V_{BTES} = \pi \cdot H_b \cdot n_{b,t} \cdot (0.525 \cdot s_b)^2 \quad (16)$$

where H_b is depth of the boreholes, $n_{b,t}$ is the total number boreholes and s_b is the distance between two adjacent boreholes. The total number of boreholes, connected in series and in parallel, can be calculated through the following product:

$$n_{b,t} = n_{b,h} \cdot n_{b,s} \quad (17)$$

where $n_{b,h}$ is the numbers of boreholes in the innermost ring of the BTES and $n_{b,s}$ is the number of boreholes in each series.

The other input parameters required for the DST are the undisturbed soil temperature $T_{s,0}$, the average thermal conductive λ_s and heat capacity $C_{p,s}$ of the soil and the borehole thermal resistance R_b of the ground-coupled heat exchangers. The latter parameter is fundamental in order to define the heat transfer within the soil through these exchangers, and in the proposed model, it was defined by the following analytical equation proposed in the literature for double-U ground-coupled heat exchangers [39]:

$$R_b = \frac{1}{8 \cdot \pi \cdot \lambda_g} \cdot \left[\ln\left(\frac{r_b}{r_{p,o}}\right) + 2 \cdot \ln\left(\frac{r_b}{\sqrt{2} \cdot x_c}\right) + \ln\left(\frac{r_b}{2 \cdot x_c}\right) - \left(\frac{\lambda_g - \lambda_s}{\lambda_g + \lambda_s}\right) \cdot \ln\left(\frac{r_b^8 - x_c^8}{r_b^8}\right) \right] + \frac{R_p}{4} \quad (18)$$

In the above equation, r_b is the radius of the borehole, $r_{b,o}$ is the outer radius of each pipe, x_c is half of the shank spacing between the U-legs, λ_g is the thermal conductivity of the grout and R_p is the thermal resistance of a single pipe . The R_p, in turn, can be calculated as the sum of the conductive thermal resistance across the pipe and the fluid-pipe convective thermal resistance, by the following expression:

$$R_p = \frac{\ln\left(\frac{r_{p,o}}{r_{p,i}}\right)}{2\cdot\pi\cdot\lambda_p} + \frac{1}{2\cdot\pi\cdot r_{p,i}\cdot h_f} \tag{19}$$

where $r_{b,i}$ is the inner radius of the pipe, λ_p is the thermal conductivity of the pipe material and h_f is the convective heat transfer coefficient between the fluid and the pipe. The latter term, in the case of a circular pipe, can be obtained from the Nusselt number as:

$$h_f = \frac{Nu\cdot\lambda_f}{2\cdot r_{p,i}} \tag{20}$$

where λ_f is the thermal conductivity of the fluid. To calculate the Nusselt number, the following correlation, valid for turbulent flow inside smooth pipes, provided by Gnielinski [40] was considered:

$$Nu = \frac{\left(\frac{f}{8}\right)\cdot(Re-1000)\cdot Pr}{1+12.7\cdot\left(\frac{f}{8}\right)^{1/2}\cdot\left(Pr^{2/3}-1\right)} \tag{21}$$

where *Re* is the Reynolds number, *Pr* is the Prandtl number and *f* is the Darcy-Weisbach frictional factor. The Reynolds number, in turn, can be calculated as:

$$Re = \frac{2\cdot m_{f,U}}{\pi\cdot r_{p,i}\cdot\mu_f} \tag{22}$$

where $m_{f,U}$ is the mass flow rate inside a single U-leg and μ_f is the dynamic viscosity of the fluid. The Prandtl number is defined as:

$$Pr = \frac{c_{p,f}\cdot\mu_f}{\lambda_f} \tag{23}$$

where $c_{p,f}$ is the specific heat of the fluid. Finally, for the friction factor the following correlation proposed by Haaland [41] was used:

$$f = \left[-1.8\cdot\log\left(\frac{\varepsilon_p}{7.4\cdot r_{p,i}}\right)^{1.11} + \frac{6.9}{Re}\right]^{-2} \tag{24}$$

where ε_p is the absolute roughness of the pipe surface. The possibility of considering the variations of R_b as a function of $m_{f,U}$ due to Eqs. 18-24, allows the model to be used for simulating the thermal response of the BTES with different fluid flow rates. During its operation, in fact, the BTES is alternatively connected both to the dish-Stirling and to the heat pumps and the total mass flow rate flowing inside the BTES ($m_{f,BTES}$) takes different values. From these different values, it is finally possible to define the different mass flow rates circulating inside each single U-leg of the thermal exchangers using the following expression:

$$m_{f,\mathrm{U}} = \left(\frac{m_{f,BTES}}{2 \cdot n_{b,h}} \right) \tag{25}$$

that was deducted considering the mass conservation equation of the fluid circulating inside the BTES. Using the above nomenclature, the thermal power that can be transferred or recovered from the BTES during its summer or winter operation is calculated from the global thermal balance of the system as:

$$\dot{Q}_{BTES} = \dot{m}_{f,BTES} \cdot c_{p,f} \cdot \left(T_{o,BTES} - T_{i,BTES} \right) \tag{26}$$

where $T_{\mathrm{o,BTES}}$ and $T_{\mathrm{i,BTES}}$ are the outlet and inlet temperatures of the BTES, respectively. Moreover, considering that during the years of operation of the system, the BTES will be subject to numerous thermal loading and unloading cycles, it is possible to calculate the total thermal energy charged into the BTES by the following integral:

$$E_{BTES,in}(n_y) = \sum_{i=1}^{n_y} \left(\int_{charge,i} \dot{Q}_{BTES} dt \right) \tag{27}$$

where n_{y} is the number of years of plant operation and *charge,i* is the interval of time during which the BTES is charged every year. Similarly, the total thermal energy recovered from the BTES can be calculated as:

$$E_{BTES,out}(n_y) = \sum_{i=1}^{n_y} \left(\int_{discharge,i} \dot{Q}_{BTES} dt \right) \tag{28}$$

where *discharge,i* is the interval of time during which the BTES is discharged every year. Using these energies, it is possible to calculate the total thermal storage efficiency of the system, after a number of years n_{y}, as

$$\eta_{BTES}(n_y) = \frac{E_{BTES,out}(n_y)}{E_{BTES,in}(n_y)} \tag{29}$$

As shown in the analysis of the results in this work, efficiency η_{BTES} was used to assess which of the proposed BTES configurations performs the best.

The calibration parameters of the model used to simulate the thermal behaviour of the BTES are summarised in Table 3. More specifically:

- the thermal characteristics of the soil are those typical of the facility test area at the University of Palermo (Sicily);
- the thermal conductivity of the grout was estimated assuming it is made with a mixture of 10% Bentonite/90% Quartzite sand [39];
- the radius of the pipes and the distances between the U-legs are those typical of the commercial products used for ground-coupled heat exchangers;
- the conductivity of the exchanger tubes is that of high-density polyethylene.

Finally, regarding the thermal properties of the water used to calculate h_f, the values corresponding to the average temperature of the fluid entering and leaving the BTES were used. All the remaining parameters of the model (such as $n_{b,h}$, $n_{b,s}$, s_b) were set to perform the optimisation analysis described below in this paper.

Table 3: Parameters defined for the BTES model

Parameters	**Value**	**Units**
Borehole depth H_b	25	m
Undisturbed soil temperature, $T_{s,o}$	18	°C
Thermal conductivity of the soil, λ_s	1.75	W/(m K)
Volumetric heat capacity of the soil, $C_{p,s}$	2.72	GJ/(m^3·K)
Thermal conductivity of the grout, λ_g	2	W/(m K)
Thermal conductivity of the pipes, λ_p	0.45	W/(m K)
Radius of the boreholes, r_b	0.075	m
Inner radius of the pipes, $r_{b,i}$	0.016	m
Outer radius of the pipes, $r_{b,o}$	0.020	m
Half shank spacing between the U-legs, x_c	0.040	m
Absolute roughness of the pipe surface, ε_p	$2\cdot10^{-5}$	m

2.3 HEAT PUMP NUMERICAL MODEL

As regards the modelling of the water-to-water heat pump system, a simple black-box model that was considered, which was defined by interpolating the operating data provided by the manufacturer [34]. The first heat pump (HP1) and the second heat pump (HP2) have a rated heating capacity of 200 kW$_{th}$ and 300 kW$_{th}$ respectively. The technical data of these pumps, for a fixed hot-side outlet temperature of $T_{h,o}$=45 °C, are summarised in Table 4, as a function of the inlet cold-side temperature of $T_{c,i}$ (ranging between $T_{c,i}$=8-20 °C). In these tables $\dot{Q}_{FH}$ is the (full-load) heating power, $\dot{Q}_C$ is the cooling power, E_H is the electric power consumption and COP_{FL} is the coefficient of performance. When the heating power demand $\dot{Q}_{PH}$ is lower than the heat power output $\dot{Q}_{FH}$ that the heat pump can provide at $T_{c,i}$, there is a degradation of the coefficient of performance due to this partialisation. In this case, the current value of the coefficient of performance can be calculated as:

$$COP_{PL} = PLF \cdot COP_{FL}(T_{h,i}) \tag{30}$$

where PLF is the partial load factor that is defined as [34], [42]:

$$PLF = \frac{PLR}{C_c \cdot PLR + (1 - C_c)} \tag{31}$$

C_c is a degradation coefficient (that is assumed equal to C_c=0.90) and *PLR* is the partial load ratio, defined as:

$$PLR = \frac{\dot{Q}_{PH}}{\dot{Q}_{FH}(T_{c,i})} \tag{32}$$

Table 4: Operating technical data of HP1 (model WW 302.B200) and HP2 (model WW 302.B300).

$T_{h,o}$= 45 °C								
$T_{c,i}$ (°C)	$\dot{Q}_{FH}$ (kW$_{th}$)		$\dot{Q}_C$ (kW$_{th}$)		$\dot{E}_{ele,hp}$ (kW$_e$)		COP_{FL}	
	HP1	HP2	HP1	HP2	HP1	HP2	HP1	HP2
8	159	248	123	191	39.1	60.2	4.07	4.12
10	175	276	139	219	39.4	60.5	4.44	4.56
15	198	306	159	248	39.8	61.0	4.97	5.02
20	221	346	182	288	40.3	61.4	5.48	5.64

From the value of the COP_{PL} (evaluated by Eqs. 30-32) it is lastly possible to calculate the electric absorption of the heat pumps. The outlet cold-side temperature from the heat pumps can be calculated as.

$$T_{c,o} = T_{c,i} - \frac{\dot{Q}_c}{\dot{m}_{c,HP} \cdot c_{p,f}} \tag{33}$$

where $\dot{m}_{c,HP}$ is the mass water flow rate at source-side of each heat pump. From technical sheets, the mass flow rates considered for the calculations are $\dot{m}_{c,HP}$=25,376 [kg/h] and $\dot{m}_{c,HP}$ =41,968 [kg/h] for the HP1 and HP2, respectively. An algorithm was implemented in the control system to minimise the partialisation of heat pump operation by alternating or parallel starting of the heat pumps as a function of the heating demand levels of the building [34].

2.4 TRANSIENT SYSTEM SIMULATION TOOL IMPLEMENTATION OF THE PLANT MODEL

The models describing the energy balance of the different components of the proposed plant were developed with reference to the literature and then numerically implemented using TRNSYS [43]. This software allowed the numerical analysis of a large number of different layout configurations to be performed through a series of transient hourly-based simulations. With this aim, the hourly data time series of the air temperature and Direct Normal Irradiance (DNI) were defined using the Typical Meteorological Year (TMY) generated by Meteonorm [44] and were used as input variables of the model.

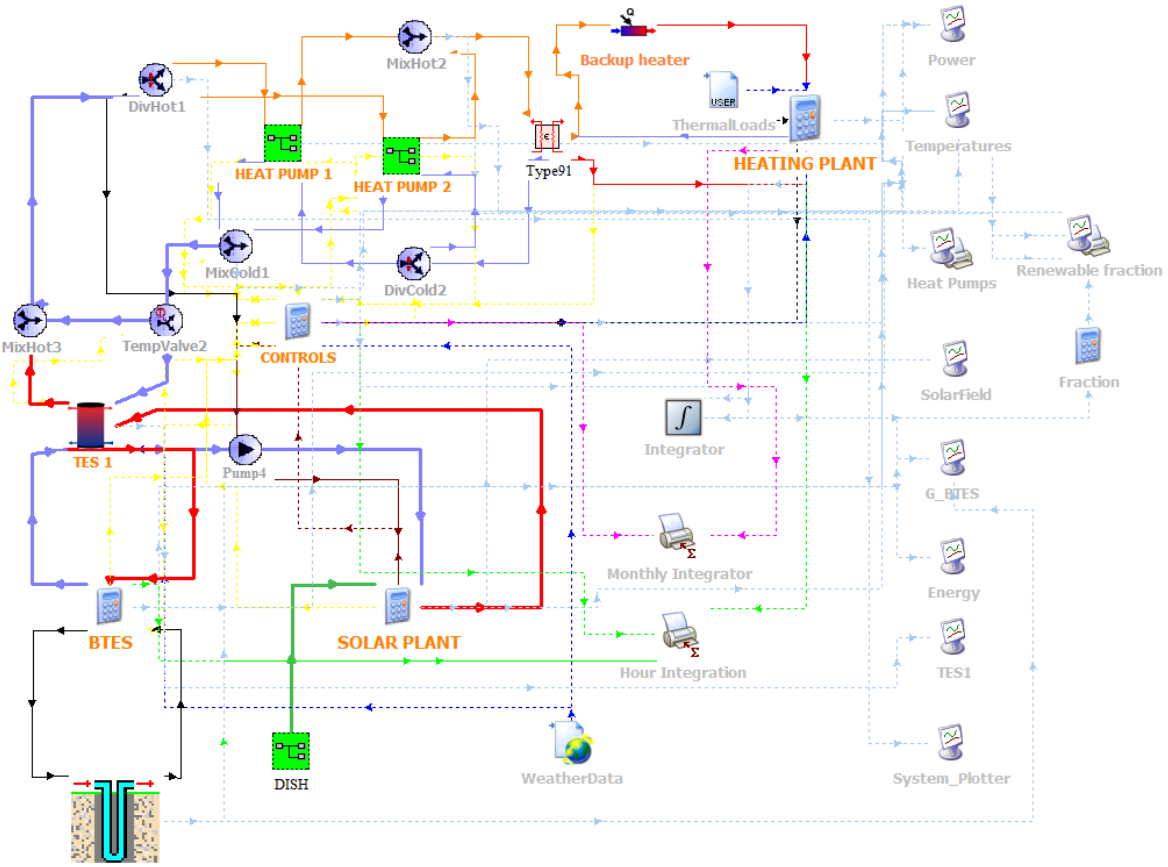

Figure 3: TRNSYS layout of the plant model.

The simulation period was set to 25 years to fully characterise the thermal evolution of the BTES from the beginning of its operation until the achievement of its pseudo-stationary condition. For each of these years the same TMY dataset was used. Figure *3* shows the structure of the TRNSYS layout in which all the connections between the different elements constituting the system were modelled (including all the valves, heat exchangers, circulation pumps, etc.). Moreover, all the equations representing the model of each plant component already described, were implemented using equation TRNSYS types and for the dish-Stirling and the heat pump, special macros were developed for this purpose.

2.5 MULTI-CRITERIA ANALYSIS

In this work, a series of different configurations of the same plant layout were studied in order to identify the one performing best one in terms of energy, environment and economics. Referring to Figure 4, the different analysed configurations were obtained by varying the following parameters that characterise the previously presented layout:

- the number of dish-Stirling units n_{dish}, (varying from 1 to 4 with a step of 1)

- the number of head boreholes $n_{b,h}$, (varying from 15 to 20 with a step of 5)
- the number of boreholes in series $n_{b,s}$, (varying from 3 to 4 with a step of 1)
- the spacing of boreholes in series s_b, (varying from 2 to 12 m with a step of 2 m)
- the deep of the boreholes H_b, (varying from 10 to 100 m with a step of 10 m).

In this way, 1440 different plant system configurations were obtained whose transient operation during their useful lifetime (25 years) was simulated using the TRNSYS numerical model. All these simulations were carried out keeping the evaluated space heating load of the building E_{load} unchanged. Each simulation generated the time variations of about 40 variables, giving rise to a result matrix characterised by 40 columns and 219000 rows. Thus, the performed simulations produced a total number of items in the result dataset equal to about $1.26 \cdot 10^{10}$. This significant amount of data required the adoption of particular manipulation techniques through the creation of a MySQL database that, properly optimised, allows the efficient management and examination of almost 57 GB of data. For each studied configuration, it was possible to calculate, from the results of the simulation, the fraction of building heating load that is covered by the thermal energy provided by the heat pump system, as:

$$f_{hp} = \frac{E_{hp}}{E_{load}} \tag{34}$$

where E_{hp} is the thermal energy produced by the two heat pumps in one year and E_{load} is the heating energy load required by the building during the same year.

Furthermore, considering that, in general, the electricity required by heat pumps is not necessarily produced from renewable sources, the following definition of annual renewable fraction was adopted for each studied configuration:

$$f_r = \frac{E_{load} - \left(E_{ele,hp} + E_{gas,boiler}\right)}{E_{load}} = f_{hp} \cdot \left(1 - \frac{1}{COP_{hp}}\right) \tag{35}$$

where $E_{ele,hp}$ is the annual electric energy absorbed by the heat pumps, $E_{gas,boiler}$ is the thermal energy annually delivered by the gas boiler backup heater and COP_{hp} is the coefficient of performance of the heat pump system. If the $E_{ele,hp}$ is fully provided by the electricity annually produced by the dish-Stirling it follows that Eq. 34 is a sufficient indicator of the annual renewable fraction of the plant.

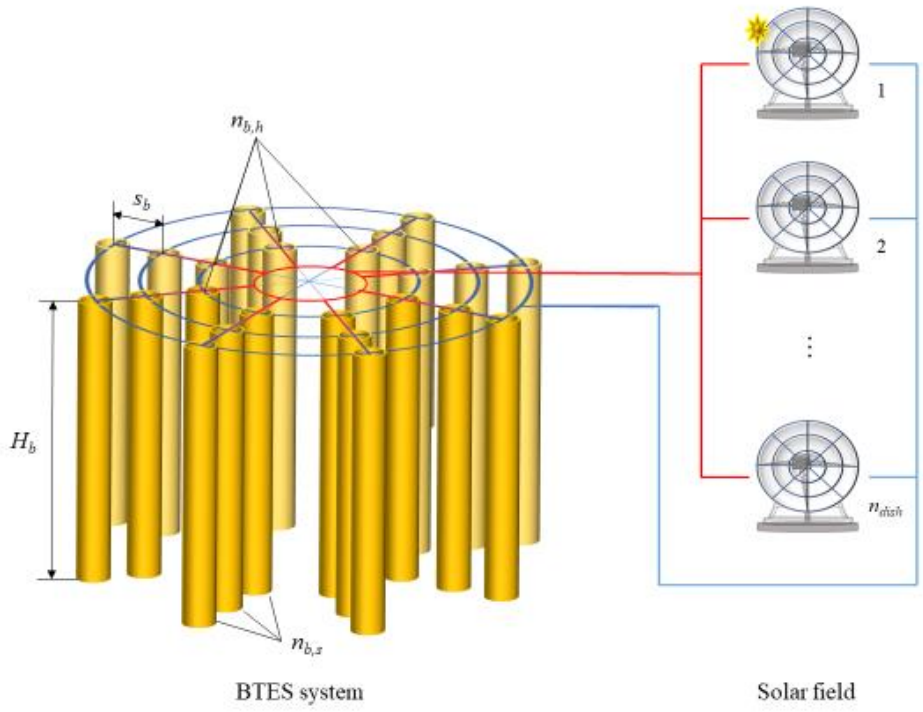

Figure 4: Decision variables of plant layout optimisation

However, even under this hypothesis, the coefficient f_r can be considered a good indicator of the more or less renewable fraction of the plant, as the higher the value of f_r, the lower the fraction of heating loads covered by the backup heater, the lower the amount of electricity absorbed by the heat pumps and, thus, the greater the fraction of electricity, produced by the solar field, left free to cover other consumption.

2.5.1 Economic analysis

Knowing the annual renewable fraction of each of the 1440 plant configurations, an economic analysis was performed taking into account several possible scenarios. According to estimates, the initial cost of investment necessary to build the entire plant consists of: the cost of a single dish-Stirling solar concentrator (C_{dish}), including installation and maintenance costs over the lifetime of the system, amounts to € 278,000; the cost of realisation of a single geothermal probe expressed per unit of length (C_{BTES}) amounts to 60 €/m; the total cost necessary to purchase the two selected water-to-water heat pumps (C_{HP}) amounts to €50,000.

The initial overall cost of investment (I) for a generic CHP configuration plant depends on the number of installed solar concentrators (n_{dish}) and the total length of boreholes L_{tot} making up the thermal storage system which is equal to the product of the total number of boreholes ($n_{b,t}$) for the depth of a single borehole (H_b). The economic analysis was conducted on the basis of a "constant currency approach" considering the plant's useful lifetime being equal to 25 years,

and the initial cash flow includes only the investment related to the examined configuration. For subsequent years, the cash flow was evaluated considering the following revenues and costs.

The incentivised sale of the electricity produced by the concentrating solar power field to the national electricity grid ($I_{el,\,sold}$). The dish-Stirling system of Palermo benefits from the national incentivisation mechanism no longer in force since December 2017 [45]. According to this decree, the feed-in tariff (T_f) is granted to a power plant with an electric capacity up to 500 kW for 25 years and is determined as follows:

$$T_f = T_b + Pr_{solar} \quad \left(\frac{€}{MWh}\right) \tag{36}$$

where, T_b is the basic incentive tariff that depends on the size of the power plant equal to 324 €/MWh, and Pr_{solar} is the bonus corresponding to the solar integration fraction that characterises the considered power plant. For the generation plant in issue, this bonus is equal to 45 €/MWh since the fraction of solar integration is 1. Overall, the feed-in tariff amounts to 369 €/MWh. The incentive for the replacement of a conventional heating plant with a new heating plant equipped with geothermal heat pumps (I_{hp}) [46]. This income has a duration of 5 years and was calculated as follows:

$$I_{hp} = P_n \cdot Q_{uf} \cdot \left(1 - \frac{1}{COP_{hp}}\right) \cdot C_t \quad \left(\frac{€}{year}\right) \tag{37}$$

Where: P_n indicates the nominal heat output of the installed heat pump expressed in kW_{th}; Q_{uf} indicates the utilisation coefficient dependent on climate zone; COP_{hp} is the coefficient of performance of the installed heat pump; and C_t is the coefficient of valorisation of the thermal energy produced expressed in €/kWh. The incentive calculated by referring to the two heat pumps planned for the cogeneration plant described in this document is:

I_{hp}=23,483.73 €/year

The natural gas savings resulting from the use of renewable heat pumps $\left(S_{natural\,gas}\right)$.

These savings are calculated as:

$$S_{natural\ gas} = E_{load} \cdot f_r \cdot \left(\frac{c_{\substack{natural \\ gas}}}{\eta_{\substack{gas \\ boiler}}} - \frac{c_{electricity}}{COP_{hp}} \right) \quad \left(\frac{€}{year} \right) \tag{38}$$

where: E_{load} is the yearly heating energy demand of the building expressed in (kWh/year); f_r is the annual renewable fraction of the examined CHP plant; $c_{\substack{natural \\ gas}}$ (0.112 €/kWh) and $c_{electricity}$ (0.170 €/kWh) are unit costs of natural gas and electricity respectively, expressed in (€/kWh); $\eta_{\substack{gas \\ boiler}}$ is overall yield of the existing gas boiler; COP_{hp} is coefficient of performance of the two renewable heat pumps.

The income resulting from the monetisation of avoided CO_2 emissions $\left(I_{CO_2} \right)$, calculated as:

$$I_{CO_2} = \frac{se_{CO_2} \cdot E_{load} \cdot f_r}{10^6} \cdot C_{CO_2} \quad \left(\frac{€}{year} \right) \tag{39}$$

where: se_{CO_2} indicates the specific emissions of CO_2 related to the thermal energy production using natural gas, expressed in (gCO_2/kWh_{th}); E_{load} is yearly heating energy demand of the building expressed in (kWh/year); f_r is the annual renewable fraction of the examined CHP plant and C_{CO_2} is the unit revenue related to the amount of CO_2 avoided expressed in (€/t_{CO2}). Ultimately, taking into account the four monetary items listed above, the cash flow for the t-th year (CF_t) for the facility can be expressed as follows:

$$CF_t = I_{el,sold} + I_{hp} + S_{natural\ gas} + I_{CO_2} \quad \left(\frac{€}{year} \right) \tag{40}$$

2.5.2 Design of new mechanism of incentivisation

In Italy there is currently no national incentive mechanism for CHP plants that exploit renewable sources by innovative technologies, such as the dish-Stirling solar concentrator. Although the energy efficiency of this technology is widely acclaimed [47], [37,48,49], the main factor limiting the spread of the dish-Stirling concentrator is the initial investment which is still too high compared to other solar technologies fully developed and marketed. Assuming that the incentive scheme described in section 5.2 can continue to be used even if the reference decrees are partly no longer in force, this document suggests a new incentive mechanism through which a percentage of the initial investment necessary for the realisation of a cogeneration project is financed. Four strategies of incentivisation are proposed, each with a

different percentage of initial investment financed: 0% (I_0), 15% (I_A), 35% (I_B) and 45% (I_C). In order to assess the economic feasibility of the proposed cogeneration plant and to identify the most robust solution, the four strategies of incentivisation were investigated by varying the discount rate. As shown in Figure *5* below, three values of discount rate were fixed obtaining 12 possible financial scenarios.

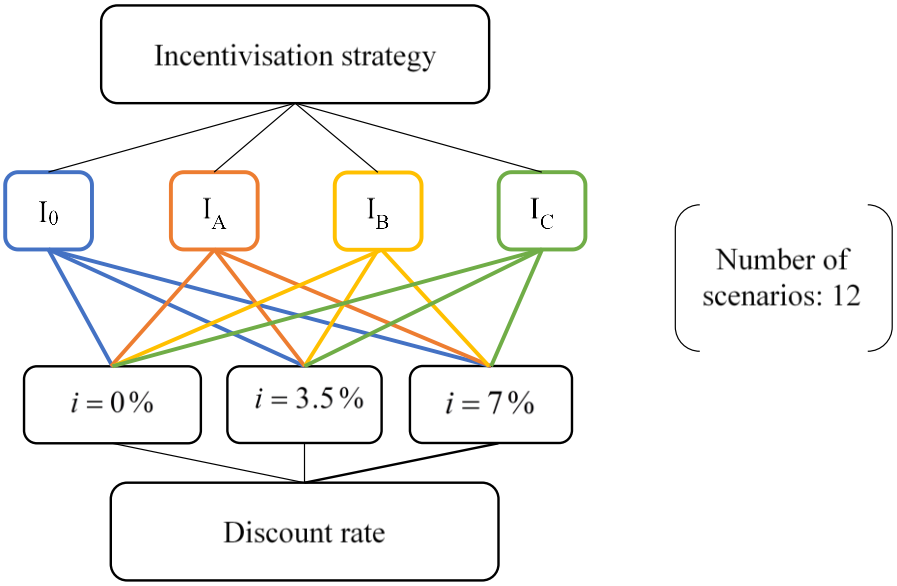

Figure 5: Schematic representation of all possible financial scenarios investigated

Referring to the 1440 plant configurations, all the financial scenarios schematically illustrated in Figure 5 were analysed by investigating several economic indicators. In particular, the Net Present Value (NPV) and the Profitability Index (PI) were calculated in order to assess the profitability of the investment; while the Discounted Payback Time (DPBT) and Internal Rate of Return were determined to assess the investment risk. The NPV and PI were calculated according to Eq. 41:

$$\begin{cases} NPV = \sum_{t=1}^{N} \frac{CF_t}{(1+i)^t} \\ PI = \frac{NPV}{I} \end{cases} \tag{41}$$

Where: CF_t is the cash flow of t-th year of the useful lifetime of project; i is the discounted rate; and I is the initial overall cost of investment. The DPBT, defined as the number of years (t) needed for the equivalent of the investment income to exceed the equivalent of the capital expenditure, was determined according to Eq. 42:

$$t \mid \sum_{t=0}^{N} \frac{CF_t}{(1+i)^t} \geq 0 \tag{42}$$

The IRR represents the percentage or interest rate (i) earned on the unrecovered part of an investment and it was calculated according to Eq. 43:

$$i \mid NPV = \sum_{t=1}^{N} \frac{CF_t}{(1+i)^t} = 0 \tag{43}$$

All these economic indicators were normalised in order to make them comparable, using the min-max normalisation as in Eq. 44:

$$z = \frac{x - min(x)}{max(x) - min(x)} \tag{44}$$

where: z is the normalised value of the set of observed values of x; $max(x)$ and $min(x)$ are maximum and minimum values of the same set of values. The obtained Boolean variables were indicated as $NPV_{normalised}$, $PI_{normalised}$ and $DPBT_{normalised}$. It was then possible to calculate the Overall Economic Viability Evaluation (OEVE) index, which graphically represents the area of a triangle whose vertices are the aforementioned economic variables as shown in Figure 6.

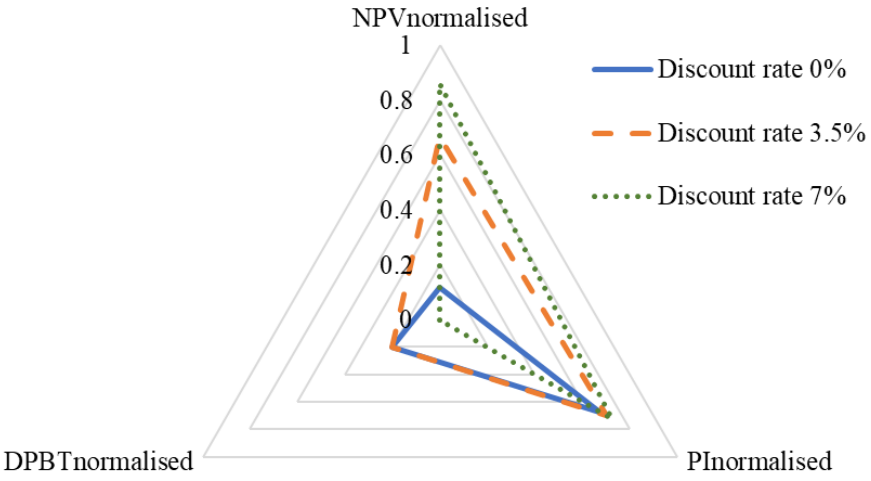

Figure 6: Radar diagram withe normalised economic indexes of the configuration ID261.

The higher the OEVE index is, (larger area in Figure 6) the more profitable the investment required to realise the corresponding CHP system configuration.

2.5.3 Evaluation of CO_2 emissions

The realisation of the CHP plant proposed and analysed in this paper would undoubtedly bring an environmental benefit in terms of avoided CO_2 emissions. The amount of CO_2 emissions avoided, which corresponds to the operation of the various optimal configurations of the CHP system can be quantified as follows:

$$AE_{CO_2} = \frac{S_{\substack{thermal \\ energy}} \cdot se_{CO_2}}{ULT} \quad \left[\frac{t_{CO_2}}{year}\right] \tag{45}$$

where: $S_{\substack{thermal \\ energy}}$ indicates the thermal energy savings, i.e. the thermal energy required by the building no longer supplied by the existing gas boiler but supplied through the renewable heat pumps over the lifetime of the CHP plant; se_{CO_2} indicates the specific emissions of CO_2 related to the thermal energy production using natural gas, expressed in (gCO_2/kWh_{th}); and ULT indicates the lifetime of the examined plant, which is 25 years in this case study.

3. CASE STUDY

As an application of the proposed methodology, reference has been made to one of the non-residential buildings of the University campus of Palermo: Building 9 of the Department of Engineering. According to the Italian standard UNI 10349 concerning climate data, Palermo falls into the B climate zone characterised by 751 Heating Degree Days (HDD) and the legal period for space heating ranges from 1 December to 31 March, for 8 hours per day [50]. Palermo has a Mediterranean climate characterised a temperate-wet winter with an average temperature range from 8 °C to 14 °C, and by a hot-dry summer with an average temperature range from 21 °C to 28 °C, with peaks of above 35-40 °C [51]. The existing heating system of the building includes two gas boilers that feed a series of radiators. The heating volume is 14,500 m^3 and there is a conventional heating system with gas boilers with a total nominal power of 600 kW. Figure 7 reports the thermal load demand of Building 9 during a typical week of each month of the conventional heating period. According to historical and measured data the monthly heating load energy demand of the considered building is: 59489 kWh in January, 38702 kWh in February, 6264 kWh in March and 62090 kWh in December. The overall yearly heating load energy demand is: E_{load}=166545 kWh. Finally, the hourly-based climate data input of the was defined using the Typical Meteorological Year (TMY) generated by Meteonorm [44] for Palermo (38.11°N; 13.36°E).

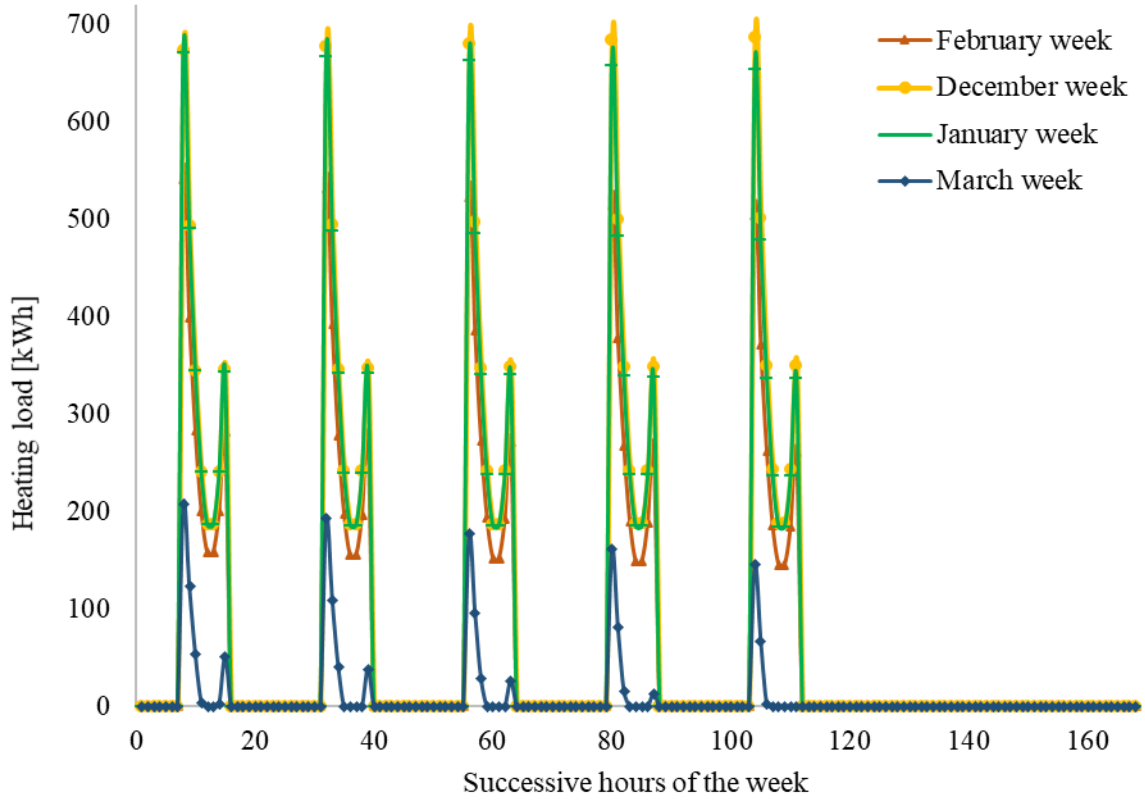

Figure 7: Weekly profile of heating load energy demand of building 9 during the conventional heating period of year

4. RESULTS AND DISCUSSION

As already described, the dish-Stirling system represents the central element of the proposed cogeneration layout.

Table 5 shows the cumulative monthly values of the electrical and thermal energies produced by a single unit located in Palermo [44]. In

Table 5, the following monthly cumulated quantities are indicated: the solar energy collected by the solar concentrator (E_{sun}), the gross and net electrical energies produced by the solar plant (E_g, E_n), the parasitic electrical absorption of the solar plant (E_p) and the thermal output energy rejected from the Stirling engine ($E_{S,out}$). In the following paragraphs Authors discuss and analyse the results more in detail.

4.1 ENERGY BALANCE OF THE COGENERATIVE PLANT

Values calculated using the numerical model of the dish-Stirling collector show a peak in energy production occurring in July. In this month, the net electric and the thermal efficiencies equal to 24% and 44%, respectively. The total annual net production of electric energy amounts to 40.8 MWh/year while the thermal energy rejected from the Stirling engine,

is about 88.7 MWh/year. The corresponding net electric and thermal annual efficiency are 20% and 44%, respectively. Since all these calculated quantities significantly depend on the direct solar irradiation, it was necessary to accurately select a *DNI* database representative of the micro-climatic conditions for the studied location. With this purpose, several solar databases were compared to each to other check whether the Meteonorm solar dataset could be representative of the *DNI* conditions of Palermo. Moreover, since the real operating data of dish-Stirling systems show that their performances can be considerably reduced by the soiling of the collector mirrors [37], for the presented calculations, an annual average cleanliness index equal to $\eta_{cle}^{ave}=0.9$ was assumed. This value was carefully defined by processing the real operational data of the dish-Stirling unit installed in Palermo, assuming the possibility of periodic washings of the collector mirrors.

Thus, taking into account both the good predictive accuracy of the proposed numerical model (already discussed with the introduction of the MAPE and ζ metrics) and the quality of the input data (DNI and average cleanliness index), it is possible to reasonably assert that the energy outputs of

Table 5 accurately represent the monthly producibility of a dish-Stirling plant located in Palermo.

Table 5: Producibility of a single dish-Stirling plant in Palermo

Month	E_{sun} (MWh)	E_g (MWh)	E_p (MWh)	E_n (MWh)	E_{th} (MWh)
January	8.99	2.30	1.19	1.11	4.07
February	8.21	2.20	1.08	1.12	3.65
March	14.28	3.87	1.19	2.68	6.32
April	15.28	4.13	1.15	2.98	6.77
May	23.23	6.44	1.19	5.25	10.19
June	24.58	6.75	1.15	5.60	10.82
July	28.65	8.03	1.19	6.84	12.51
August	22.60	6.18	1.19	4.99	9.97
September	17.84	4.90	1.15	3.75	7.86
October	15.10	4.14	1.19	2.94	6.66
November	12.31	3.32	1.15	2.17	5.46
December	9.94	2.63	1.19	1.44	4.44
Annual	**201.01**	**54.88**	**14.02**	**40.87**	**88.72**

As already mentioned, to eliminate this temporal mismatch, a BTES was introduced into the plant layout. In order to show the annual energy balance of the proposed layout and the energy fluxes between its different components, the data from the simulation results relative to a representative plant configuration is described below. This studied configuration (ID90), is one of the best performing among all that have been analysed using the multi-criteria optimisation process and is characterised by the following geometrical parameters:

- the number of dish-Stirling units n_{dish}=2
- the number of head boreholes $n_{b,h}$, =25
- the number of boreholes in series $n_{b,s}$=4
- the spacing of boreholes in series s_b=6 m
- the depth of the boreholes H_b=60 m.

For this configuration, the daily average values of the BTES soil temperature and the cumulative input and output thermal energies corresponding to a simulation period of 25 years are depicted in Figure 8.The input energies to BTES are those supplied by the solar system during the charging stages while the output energies are those transferred from the BTES to the evaporators of the heat pump system during the discharge stages. From the results of Figure 8, it is possible to observe that the average soil temperature increases during the successive years of plant operation until it reaches a pseudo-stationary condition at around the 25th year. This gradual soil temperature increase is related to the fact that the annual amount of thermal energy produced by the two solar collectors, and then stored in the BTES, is greater than the energy demanded by the heat pumps.

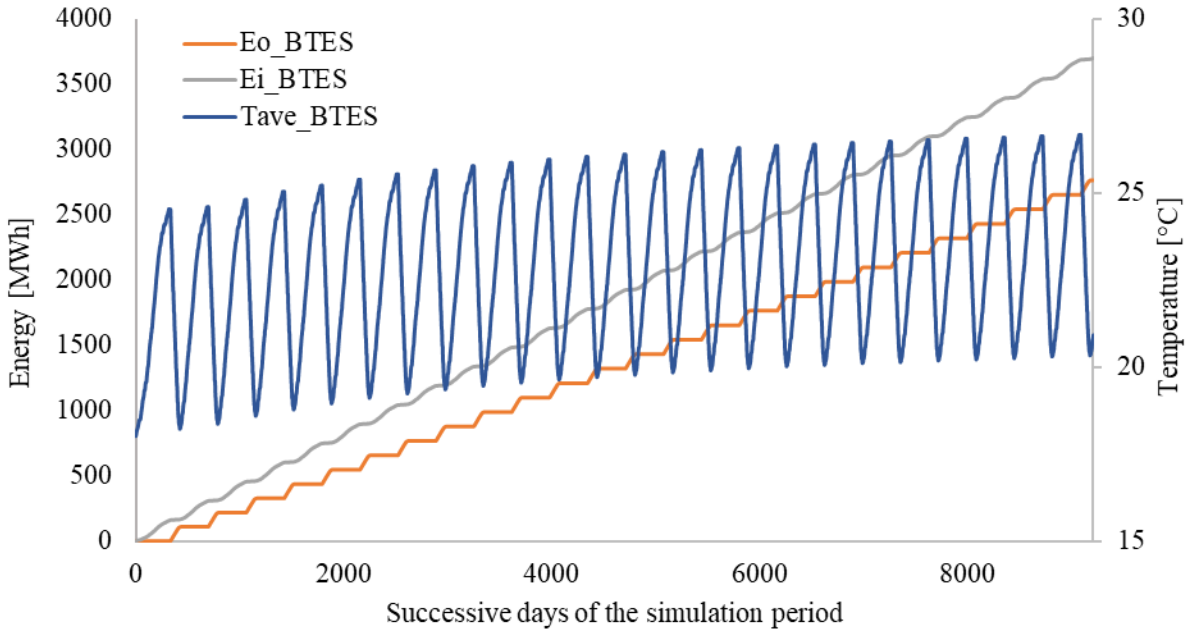

Figure 8 : average BTES temperature and cumulative input and output energy exchanged by the boreholes during the 25th year of operations (ID90 configuration)

From these results, it is also possible to calculate that the storage efficiency of the BTES reaches a value of about η_{BTES}=0.75 at the end of the studied period. This inefficiency is due both to the variations in the internal energy of the BTES soil volume (which results in the increase of the average soil temperature) and to the thermal losses from the boundaries of the same volume. These thermal losses are clearly proportional to the difference between the average temperatures of the BTES and the surrounding soil. When the system reaches its stationary configuration, at around the 25th year, the difference between the energies annually entering and leaving the BTES essentially equal its thermal losses.

The thermal energy balance of the plant during its 25th year of operation can be verified using the monthly energy values that have been summarised in Table 6. These energies are: the space heating loads of the building (E_{load}), the waste heat from the solar collector ($E_{S,out}$), the input and output energies of the BTES ($E_{BTES,in}$, $E_{BTES,out}$), the heat delivered to the heat pump evaporators ($E_{e,HP}$), the heat supplied by heat pumps to the building heating system ($E_{c,HP}$) and the energy provided by the backup heater ($E_{gas\ boiler}$). The data in Table 6 show that during the months when there is no heating demand from the building and the availability of the solar resource is greater, the waste heat from the two solar collectors is totally transferred to the BTES. This energy, for the studied configuration, amounts to $E_{S,out}$=140.33 MWh and, as already mentioned, corresponds to about 80% of annual thermal energy produced by the solar

collectors (equal to $E_{S,out}$=177.21 MWh). In the winter season, 86% of heat energy required by heat pumps for their operation ($E_{e,HP}$=133.33 MWh) is recovered from the soil ($E_{BTES,out}$=115.12 MWh) while the remaining 14% is directly supplied from the solar system ($E_{S,out}$=18.21 MWh). The residual energy produced in this period of the year by the solar systems is directly transferred into the BTES ($E_{BTES,in}$ =18.67 MWh). The latter energy represents about 11% of the thermal energy that annually charges the geothermal storage. These results show an interesting aspect of the operation of the proposed system: during the winter season it is often possible that days with clear skies occur. During these days, the direct solar irradiation levels may be sufficient for the activation of the solar collectors. Thus, if this energy collection is contemporary with the building heating demand hours, it can be directly delivered to the heat pump evaporators. Otherwise, for example at weekends, it can be stored in the BTES as during the summer season. Finally, from the data of Table 6, it is possible to observe that the studied configuration of the proposed systemis able to cover up to 97% of the annual heating demand of the building (E_{load}=166.55 MWh) while the remaining 3% is covered by the energy delivered by the gas boiler backup heater ($E_{gas\ boiler}$=5.45 MWh).

Table 6: Monthly values of the thermal energies at 25th year (ID90 configuration)

Month	E_{load} (MWh)	$E_{S,out}$ (MWh)	$E_{BTES,in}$ (MWh)	$E_{BTES,out}$ (MWh)	$E_{e,HP}$ (MWh)	$E_{c,HP}$ (MWh)	$E_{gas\ boiler}$ (MWh)
January	59.49	8.10	2.87	41.95	47.21	56.98	2.58
February	38.70	7.29	3.09	27.63	31.85	38.62	0.10
March	6.26	12.63	9.80	2.22	4.97	6.13	0.14
April	0	13.51	13.53	0	0	0	0
May	0	20.39	20.34	0	0	0	0
June	0	21.62	21.59	0	0	0	0
July	0	25.01	24.96	0	0	0	0
August	0	19.93	19.91	0	0	0	0
September	0	15.68	15.67	0	0	0	0
October	0	13.29	13.27	0	0	0	0
November	0	10.88	10.87	0	0	0	0
December	62.09	8.86	2.91	43.33	49.31	59.51	2.63
25th year	**166.55**	**177.21**	**158.79**	**115.12**	**133.33**	**161.24**	**5.45**

The electric energy balance of the plant during its 25th year of operation can be verified using the monthly energy values that have been summarised in Table 7, where are described: the net electric energy produced by the dish-Stirling plant (E_n), the electric energy absorbed by the heat pump system ($E_{ele,hp}$), the parasitic electric absorptions of the plant ($E_{plant,p}$), the net electricity

exchanged with the grid ($E_{ele,net}$), the coefficient of performance of the heat pumps (COP_{hp}) and the global coefficient of performance considering all the parasitic electric consumptions of the plant (COP).

Table 7: Monthly values of the electric energies at 25th year (ID90 configuration)

Month	E_n (MWh)	$E_{ele,hp}$ (MWh)	$E_{plant,p}$ (MWh)	$E_{ele,net}$ (MWh)	COP_{hp} (-)	COP (-)
January	2.21	10.33	0.87	-9.00	5.51	5.08
February	2.24	7.15	1.07	-5.98	5.40	4.70
March	5.37	1.24	0.56	3.57	4.94	3.40
April	6	0.00	0.38	6	0	0
May	11	0.00	0.45	10	0	0
June	11	0.00	0.46	11	0	0
July	14	0.00	0.49	13	0	0
August	10	0.00	0.46	10	0	0
September	7	0.00	0.39	7	0	0
October	6	0.00	0.38	6	0	0
November	4	0.00	0.35	4	0	0
December	2.89	10.79	0.90	-8.80	5.51	5.09
25th year	**81.73**	**29.52**	**6.75**	**45.46**	**5.46**	**4.45**

The analysis of the results of Table 7, shows that the heat pumps reach an annual COP_{hp}=5.51 which reduces to COP=4.4 if all the parasitic consumptions related to operations of the hydraulic circulators of the plant are considered. The interesting result from this data is that, considering the electric grid as an energy storage system, 44% of the electric energy annually produced by the solar field can be used to cover the total electric consumptions of the heating plant (36.27 MWh). The remaining 56% (amounting to 45.46 MWh) can, for example, be used either to cover the remaining electricity consumption of the building or simply be sold to the electric national grid. Under these assumptions, the renewable fraction of the heating system would reach the extremely high value of f_r=97 % which would correspond to a total annual reduction of emissions of $\Delta e_{CO_2} = 96\%$.

These very high values of the system efficiency were achieved through the optimisation process of the BTES geometry. In this regard, the BTES inlet and outlet temperatures and the average soil temperature are depicted in Figure 9 as a function of the successive days of the 25th year of plant operation.

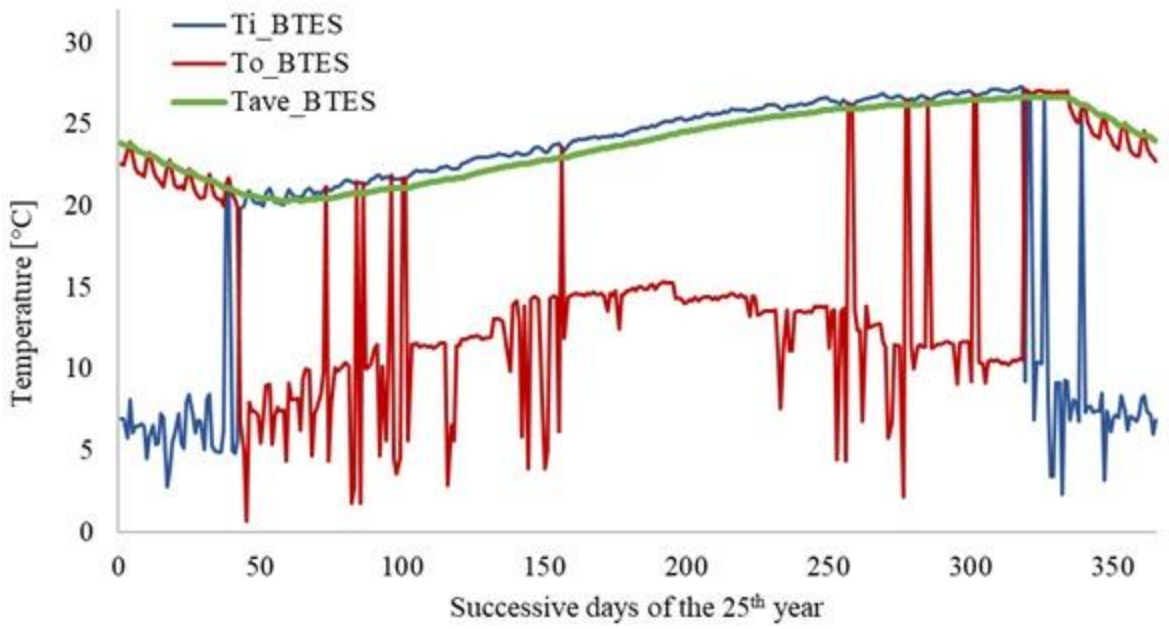

Figure 9: daily averaged values of the input, output and soil temperatures of the BTES at the 25th year of operation (ID90 configuration)

As is shown in Figure 9, during the winter discharging phases, the temperature of the fluid exiting the BTES (red line) is always higher than the inlet temperature (blue line). During the charging phase, instead, this situation is reversed. The large temperature differences of the outlet and inlet temperature with respect to the average soil temperature (green line), during the discharging and charging phases respectively, indicate the generation of local high thermal gradients around the boreholes of the BTES.

The results generated by the numerical model and presented above asses both the technical feasibility and the efficiency of the proposed CHP plant if it were located in a central Mediterranean location. However, it was not possible to compare the accuracy of these numerical results with experimental data, since there are no pilot installations of this kind currently built. To overcome this problem, the accuracy of the solutions of each individual plant component was assessed, assuming that this was sufficient to demonstrate the accuracy of the overall model. Detailed information on the calibration of the dish-Stirling model and its predictive capability has already been provided in this work, while regarding the accuracy of the BTES model, which represents the second key element of the proposed layout, it is possible to provide the following additional information:

1) the TRNSYS Type 557 was used to study the dynamic response of different BTES configurations. This Type implements the widely used Duct Ground Heat Storage Model (DST), which is considered state-of–the-art for these kinds of simulations [52]
2) the values of the soil thermal properties that were used as input for the DST model have a narrow range of possible variations which, therefore, would not lead to substantial changes in the numerical results of the simulations presented in this work.

4.2 ANALYSIS OF THE OPTIMISED COMBINED HEAT AND POWER SYSTEM CONFIGURATIONS

Through the optimization process 4 configurations were selected among the 1440 analysed. The best performing cases were selected by extracting from the dataset the configurations that maximise either the OEVE index or the ratio f_r. The first group represents the most economically advantageous configurations, while the second represents those characterised by a higher fraction of energy covered by a renewable source. The results of this process are summarised in Table 8, where the configuration identification number, the OEVE and f_r. indexes, the BTES geometric parameter, the system COP and the corresponding storage efficiency are reported. This data shows that optimised configurations refer to systems layout with a maximum of two dish-Stirling collectors. This is essentially related to the fact that both the thermal energy generated by two collectors is more than sufficient to cover the thermal loads required by the heat pumps and the number of the collectors significantly affects the investment cost required to build the system.

Table 8: selected optimum CHP system configurations

Criteria:	**highest renewable fraction**		**most cost-efficient**	
Simulation ID number	236	90	261	397
OEVE	13.15	0.15	**21.50**	**11.26**
f_r	**0.59**	**0.78**	0.43	0.72
n_{dish}	1	2	1	2
s_b (m)	8	2	12	12
$n_{b,s}$	4	4	4	3
$n_{b,h}$	15	25	20	15
H_b (m)	30	60	10	50
L_{tot} (m)	1800	6000	800	2250
V_{BTES} (m^3)	99752	20782	99752	280552
COP_{hp}	4.14	5.37	4.44	4.48
COP	3.56	4.43	3.72	3.90

f_{hp}	0.78	0.96	0.55	0.92
η_{BTES}	0.99	0.75	0.52	0.60

Moreover, the analysis of data in Table 8 suggests a second relevant observation: for a fixed number of solar collectors the configurations that are more economically advantageous (ID261 and ID397) are those with the lowest fraction of energy covered by the renewable energy source (ID236 and ID90). This trade-off can be easily explained, since: the higher the value of L_{tot} the higher the f_r ratio and the lower the OEVE index (since the investment cost of the BTES is higher). The most cost-effective configuration, for example, is the ID261 which refers to a layout with a single collector and is characterised by an f_r =0.43 and a renewable fraction equal to f_{hp}=0.55. The configuration ID90 with two solar collectors (whose results have already been discussed in detail above) is characterised, instead, by the highest renewable fraction (f_{hp} =0.96) while presents the lowest value of the OEVE index among all the others. To conclude the discussion of these results, it is interesting to underline that the configurations with two solar collectors are those that are characterized by higher COP_{hp} values compared to those with one solar collector. The higher efficiency of the former is due to the instance where the surplus of thermal energy, with respect to the heat pump demand, determines a greater increase of the BTES temperature during the charging stages. This higher soil thermal level determines a greater efficiency of the heat pumps when the BTES is discharged.

More specifically, with regard to the environmental indicators of the 4 optimum configurations, with respect to the case of a conventional heating system powered by a gas boiler, reference can be made to the quantities shown in Table 9.

Table 9: environmental indicators of the optimum configurations

Simulation ID number	$S_{thermal\ energy}$	AE_{CO_2}	Δe_{CO_2}
	(MWh/year)	(t_{CO2}/year)	(%)
261	91.4	18.4	54.9
236	129.6	26.1	77.8
397	153.2	30.9	92.0
90	159.9	32.2	96.0

From the analysis of these quantities it can be deduced that the installation of the proposed CHP plant would result in percentage emission reductions, compared to the conventional plant, ranging from 55% (for the ID261) to 96% (for the ID90). The configuration with the highest f_r ratio (ID90) would allow savings of almost 160 MWh produced from fossil per year.

With regard to the financial analysis, the DPBT values for the 4 analysed configurations, according to the 12 hypothesised financial scenarios, have been reported in Table 10. From this data, it is possible to notice that, for all the 4 configurations, assuming both a discount rate of 7% and no initial investment financing (financial scenario I_0), the incentivised sale of electricity produced by the CHP plant would not be sufficient to amortise the investment costs within 25 years (i.e. the useful life of the cogeneration plant).

Table 10: DPBT of the optimum configurations

Number of simulation	I_0	I_A	I_B	I_C	Discount rate
261	11.2	8.8	5.6	4.5	0%
	15.2	11.4	6.9	5.0	3.5%
	25	16.7	8.9	6.2	7%
236	12.0	9.6	6.4	4.9	0%
	16.6	12.6	7.9	5.9	3.5%
	25	19.2	10.3	7.3	7%
397	14.2	11.7	8.4	6.7	0%
	20.5	15.8	10.4	8.1	3.5%
	25	25	14.2	10.3	7%
90	18.9	15.7	11.4	9.3	0%
	25	25	15.2	11.8	3.5%
	25	25	25	16.8	7%

This, obviously, would represent the worst possible scenario. If, on the other hand, Authors considered an initial investment financing of 35% (scenario I_B), the payback times of the configurations with one and two concentrators would be reduced by 10 and 15 years, respectively. Assuming the same scenario I_B, the investment risk for most of the 4 configurations analysed would be significantly reduced compared to the worst-case scenario, as shown by the IRR data reported in Table 11.

Table 11: IRR of the optimum configurations

	Simulation ID number			
Scenario	236	90	261	397
I_0	6.07%	2.20%	6.67%	4.70%
I_A	8.21%	3.80%	8.96%	6.55%
I_B	12.43%	6.80%	13.53%	10.12%
I_C	15.64%	8.97%	17.03%	12.75%

It is, also, reasonable to assume that the necessary reduction in the initial investment costs (i.e. 40%) must not be exclusively related to the financing mechanism (included in the incentive scheme), but also to a possible cost reduction in the technology itself. Such as reduction could result because greater commercial diffusion of these systems could trigger economies of scale. Dish-Stirling collectors, for example, although the most efficient among all the solar systems, have not yet reached commercial maturity comparable to that of the other CSP systems.

5. CONCLUSIONS

In this work, a heat and electric power cogeneration plant that combines a field of dish-Stirling collectors, a seasonal geothermal storage and a system of water-to-water heat pumps is proposed for the first time. The cogeneration plant has been designed both to supply thermal energy to the heating system of a non-residential building and to produce electricity. The operation of the plant has been tested by means of hourly-based numerical simulations that have been carried out using a numerical model implemented with TRNSYS. Building 9 of the Department of Engineering on the Palermo University campus was used as a case study and the real operational data of a pilot dish-Stirling collector, located in the same area, was used to carefully calibrate the numerical model. Using energy and economic performance indicators, it was, finally, possible to optimise both the number of solar collectors and the geometry of the seasonal thermal storage. The best performing configuration consists of two dish-Stirling collectors and 100 geothermal exchangers, each 60 m long and 2 m apart. The two solar collectors annually generate 82 MWh of electrical energy and 177 MWh of thermal energy. 80% of the thermal energy annually produced by the Stirling engines is stored in the soil since it is generated in summer, when the heating system of the building is off. 75% of this stored energy is, then, recovered during the winter season and transferred to the evaporators of the heat pumps. 14% of all heat energy annually required by the heat pumps is directly supplied by the solar collectors whenever the energy generation is simultaneous with the heating demands of the building. With this configuration, the heat pump system can cover about 97% of the total heating demand of the building which annually amounts to 166 MWh. The annual average value coefficient of performance of the heat pump systems is equal to 5.37, while that of the whole plant, considering all the electric consumptions, is equal to 4.43. Under these conditions, if it is further assumed that the electric grid is used as a seasonal storage, it would be possible to cover all the electric requests from the heat pump employing about 44% of the total electric energy produced by the solar field during one year. In this way, a very high value, about 96%, of

thermal energy for heating the building from renewable sources could be achieved which would correspond to annual savings of 32 t_{CO2}. In addition, there would remain about 45 MWh/year of electric energy produced by the solar system that could be used either to cover all the other consumptions of the building or be sold to the national electric grid. Thus, the results of this model demonstrate the technical feasibility of the new proposed cogeneration layout by also quantifying the thermal and electrical efficiency values for a plant built in the Southern Mediterranean basin. However, further economic analyses, based on a plant's useful lifetime of 25 years, show that the commercial penetration of these types of systems should be strongly supported by a national incentive scheme capable of including both a feed-in tariff of about 369 €/MWh and an initial investment financing of at least 40%. Then, a greater commercial penetration could trigger economies of scale capable to reduction in the installation cost of the plant itself. Dish-Stirling collectors, for example, although are the most efficient among all the solar systems, have not yet reached commercial maturity comparable to that of the other CSP systems.

NOMENCLATURE

a_1	first parameter of the Stirling engine mechanical efficiency curve (Eq. 6)
a_2	second parameter of the Stirling engine mechanical efficiency curve (Eq. 6) [W]
AE_{CO_2}	amount of avoided CO_2 emissions [ton/year]
A_n	net effective surface area of the dish collector [m^2]
A_r	receiver aperture area [m^2]
C_{BTES}	unit cost of geothermal well [€/m]
C_{CO_2}	unit revenue related to the amount of CO_2 avoided [€/t_{CO2}]
C_c	degradation coefficient of the heat pump [-]
C_{dish}	unit cost of the dish-Stirling solar concentrator [€/concentrator]
$c_{electricity}$	unit cost of electricity [€/kWh]
CF_t	cash flow for the t-th year [€/year]
C_{HP}	total cost of the two selected water-to-water heat pumps [€/m]
C_i	valorisation coefficient of the thermal energy produced [-]
$c_{natural\ gas}$	unit cost of natural gas [€/kWh]
COP_{hp}	coefficient of performance of the heat pumps system [-]

COP	global coefficient of performance of the CHP plant [-]
COP_{FL}	full-load coefficient of performance of the heat pump [-]
COP_{PL}	partial-load coefficient of performance of the heat pump [-]
$C_{\mathrm{p,s}}$	volumetric heat capacity of the soil [W/(m^3·K)]
$c_{\mathrm{p,f}}$	specific heat of the heat transfer fluid in the pipes [W/(kg·K)]
$E_{BTES,\ in}$	thermal energy charged into the BTES [kWh]
$E_{BTES,\ out}$	thermal energy discharged from the BTES [kWh]
$E_{\mathrm{c,HP}}$	heat supplied by the heat pumps condensers [kWh]
$E_{\mathrm{e,HP}}$	heat delivered to the heat pump evaporators [kWh]
$E_{ele,hp}$	electric power absorption of the heat pump [W]
$E_{\mathrm{ele,net}}$	net electricity exchanged between the CHP plant and national electric grid [kWh]
E_g	gross electric power output of the CSP collector [W]
$E_{gas,boiler}$	thermal energy produced by the gas boiler [W]
E_{hp}	thermal energy produced by the two heat pumps [kWh]
E_{load}	heating energy demand of the building [kWh]
E_n	net electric power output of the CSP collector [W]
E_p	parasitic electric absorption of the system [W]
E_p^{ave}	average value of the parasitic electric absorption of the system [W]
$E_{\mathrm{plant,p}}$	parasitic electric absorptions of the CHP plant [kWh]
E_{sun}	solar energy collected by the concentrator [kWh]
$E_{S,out}$	thermal energy produced by the concentrator [kWh]
f	Darcy-Weisbach frictional factor [-]
f_r	annual renewable fraction [%]
h_{f}	convective fluid-to-pipe heat exchange coefficient [W/(m^2·K)]
h_{r}	convective heat exchange coefficient of the receiver [W/(m^2·K)]
H_{b}	deep of the boreholes of the BTES [m]
i	discount rate [%]
I	total initial investment of CHP plant [€]
I_{b}	solar beam radiation [W/(m^2)]
I_{CO_2}	income from the amount of avoided CO2 emissions [€/year]
$I_{el,\ sold}$	income from the incentive sale of renewable electricity [€/year]

I_{hp}	income from the installation of renewable heat pumps [€/year]
L_{tot}	total length of boreholes [m]
M	median function
$\dot{m}_{c,HP}$	cold-side mass flow rate of the heat pump [kg/s]
$\dot{m}_{f,BTES}$	mass flow rate of the fluid inside the U-leg exchanger [kg/s]
$\dot{m}_{f,U}$	mass flow rate of the fluid inside the U-leg exchanger [kg/s]
n	pair number of predicted values and actually measured values
$n_{b,h}$	number of boreholes in the innermost ring of the BTES [-]
$n_{b,s}$	number of boreholes in each series of the BTES [-]
$n_{b,t}$	total number of boreholes of the BTES [-]
n_{dish}	number of dish-Stirling solar concentrator [-]
Nu	Nusselt number of the heat transfer fluid in the pipes [-]
PLF	Partial load factor of the heat pump [-]
PLR	Partial load ratio of the heat pump [-]
P_n	Nominal heat output of the heat pump [W]
Pr	Prandtl number of the heat transfer fluid in the pipes [-]
Pr_{solar}	bonus corresponding to the solar integration fraction of plant [€/MWh]
Q	accuracy ratio
$\dot{Q}_{BTES}$	heat power exchanged with the BTES [W]
$\dot{Q}_C$	cooling power of the heat pump [W]
$\dot{Q}_{FH}$	full-load heating power of the heat pump [W]
$\dot{Q}_{PH}$	current heating power of the heat pump [W]
$\dot{Q}_{r,in}$	heat power absorbed by the receiver [W]
$\dot{Q}_{r,out}$	heat loss power from the receiver [W]
$\dot{Q}_{S,in}$	thermal input power of the Stirling engine [W]
$\dot{Q}_{S,out}$	thermal output power of the Stirling engine [W]
Q_{uf}	utilisation coefficient of the heat pump[-]
Re	Reynolds number of the heat transfer fluid in the pipes [-]
r_b	radius of each borehole of the BTES [m]
$r_{p,i}$	inner radius of each pipe of the U-leg thermal exchanger [m]
$r_{p,o}$	outer radius of each pipe of the U-leg thermal exchanger [m]

R_b	thermal resistance of the borehole [(m·K)/W]
R_p	total thermal resistance of a pipe of the U-leg thermal exchanger[(m·K)/W]
R_T	temperature correction factor of Eq. 6 [-]
se_{CO_2}	specific emission of CO_2 [gCO_2/kWh_{th}]
s_b	spacing between boreholes [m]
$S_{natural\ gas}$	natural gas savings [€/year]
$S_{\substack{thermal \\ energy}}$	thermal energy savings of building [kWh_{th}]
T_{air}	temperature of the air [°C]
$T_{ave,BTES}$	inlet temperature to the BTES [°C]
T_b	basic incentive tariff [€/MWh]
$T_{c,i}$	cold-side inlet temperature to the heat pump [°C]
$T_{c,o}$	cold-side outlet temperature from the heat pump [°C]
T_f	feed-in tariff [€/MWh]
$T_{h,i}$	hot-side inlet temperature to the heat pump [°C]
$T_{h,o}$	hot-side outlet temperature from the heat pump [°C]
$T_{i,BTES}$	inlet temperature to the BTES [°C]
$T_{o,BTES}$	outlet temperature from the BTES [°C]
T_r	temperature of the receiver [°C]
T_0	reference temperature [°C]
$T_{s,0}$	undisturbed temperature of the soil [°C]
T_{sky}	apparent sky temperature [°C]
ULT	lifetime of the plant [year]
V_{BTES}	conventional volume of the BTES [m^3]
W_S	mechanical output power of the Stirling engine [W]
x_c	half of the shank spacing between U-legs [m]
x_i	actually measured value of the *i*-th pair
y_i	predicted value of the *i*-th pair

Greek letters

Δe_{CO_2}	total annual reduction of emissions [%]
ε_p	absolute roughness of the pipe surface [m]

ε_r	emissivity of the receiver [-]
ζ	median symmetric accuracy
$\eta_{\substack{gas \\ boiler}}$	overall yield of the existing gas boiler [-]
η_{BTES}	storage efficiency of the BTES [-]
η_{cle}	cleanliness index of the collector mirrors [-]
η_{cle}^{ave}	average value of the cleanliness index of the collector mirrors [-]
η_e	electrical efficiency of the alternator [-]
η_o	optical efficiency of the collector with clean mirrors [-]
$\eta_{S,M}$	mechanical efficiency of the Stirling engine [-]
$\eta_{S,T}$	thermal efficiency of the Stirling engine [-]
λ_f	thermal conductivity of the heat transfer fluid [W/(m·K)]
λ_g	thermal conductivity of the borehole grout [W/(m·K)]
λ_p	thermal conductivity of the pipe material [W/(m·K)]
λ_s	average thermal conductivity of the soil [W/(m·K)]
μ_f	dynamic viscosity of the fluid [kg/(m·s)]
σ	Stefan-Boltzmann constant, $5.67 \cdot 10^{-8}$ [W/(m^2·K^4)]

Acronyms

ATES	Aquifer Thermal Energy Storage
BTES	Boreholes Thermal Energy Storage
CHP	Combined Heat and Power
CO_2	Carbon dioxide
COP	Coefficient of Performance of a heat pump
CSP	Concentrating Solar Power
DNI	Direct Normal Irradiance
DPBT	Discounted Payback Time
DST	Duct Ground Heat Storage Model
GHG	Greenhouse Gases
GHI	Global Horizontal Irradiance
GWTES	Gravel-Water thermal energy storage
HDD	Heating Degrees Days
HP	Heat Pump

HWTES	Hot Water Thermal Energy Storage
IRR	Internal Rate of Return
MAPE	Mean Absolute Percentage Error
NPV	Net Present Value
OEVE	Overall Economic Viability Evaluation
PCU	Power Conversion Unit
PI	Profitability Index
RES	Renewable Energy Sources
STES	Seasonal Thermal Energy Storage
STTES	Short-Term Thermal Energy Storage
TMY	Typical Meteorological Year

REFERENCES

[1] World Meteorological Organization. The Global Climate in 2015 - 2019. Cent Res Epidemiol Disasters Natl Inst Sp Res 2016:32.

[2] D'Amico A, Ciulla G, Traverso M, Lo Brano V, Palumbo E. Artificial Neural Networks to assess energy and environmental performance of buildings: An Italian case study. J Clean Prod 2019;239. doi:10.1016/j.jclepro.2019.117993.

[3] Hurwitz ZL, Dubief Y, Almassalkhi M. Economic efficiency and carbon emissions in multi-energy systems with flexible buildings. Int J Electr Power Energy Syst 2020;123:106114.

[4] Ciulla G, D'Amico A, Lo Brano V, Traverso M. Application of optimized artificial intelligence algorithm to evaluate the heating energy demand of non-residential buildings at European level. Energy 2019;176:380–91. doi:10.1016/j.energy.2019.03.168.

[5] Esen M, Yuksel T. Experimental evaluation of using various renewable energy sources for heating a greenhouse. Energy Build 2013;65:340–51.

[6] Lund H. Renewable energy strategies for sustainable development. Energy 2007;32:912–9. doi:https://doi.org/10.1016/j.energy.2006.10.017.

[7] Kousksou T, Bruel P, Jamil A, Rhafiki] T [El, Zeraouli Y. Energy storage: Applications and challenges. Sol Energy Mater Sol Cells 2014;120:59–80. doi:https://doi.org/10.1016/j.solmat.2013.08.015.

[8] Mazzoni S, Ooi S, Nastasi B, Romagnoli A. Energy storage technologies as techno-economic parameters for master-planning and optimal dispatch in smart multi energy

systems. Appl Energy 2019;254. doi:10.1016/j.apenergy.2019.113682.

[9] Singh UR, Kumar A. Review on solar Stirling engine: Development and performance. Therm Sci Eng Prog 2018;8:244–56. doi:10.1016/j.tsep.2018.08.016.

[10] Buscemi A, Panno D, Ciulla G, Beccali M, Lo Brano V. Concrete thermal energy storage for linear Fresnel collectors: Exploiting the South Mediterranean's solar potential for agri-food processes. Energy Convers Manag 2018;166:719–34. doi:10.1016/j.enconman.2018.04.075.

[11] Beltagy H, Semmar D, Lehaut C, Said N. Theoretical and experimental performance analysis of a Fresnel type solar concentrator. Renew Energy 2017;101:782–93.

[12] Khan J, Arsalan MH. Solar power technologies for sustainable electricity generation – A review. Renew Sustain Energy Rev 2016;55:414–25. doi:https://doi.org/10.1016/j.rser.2015.10.135.

[13] Coventry J, Andraka C. Dish systems for CSP. Sol Energy 2017;152:140–70. doi:10.1016/j.solener.2017.02.056.

[14] Reddy] V [Siva, Kaushik SC, Ranjan KR, Tyagi SK. State-of-the-art of solar thermal power plants—A review. Renew Sustain Energy Rev 2013;27:258–73. doi:https://doi.org/10.1016/j.rser.2013.06.037.

[15] Desideri U, Zepparelli F, Morettini V, Garroni E. Comparative analysis of concentrating solar power and photovoltaic technologies: Technical and environmental evaluations. Appl Energy 2013;102:765–84. doi:https://doi.org/10.1016/j.apenergy.2012.08.033.

[16] Meyer R, Schlecht M, Chhatbar K. Solar resources for concentrating solar power (CSP) systems. Conc Sol Power Technol 2012:68-e2. doi:10.1533/9780857096173.1.68.

[17] Ferreira AC, Nunes ML, Teixeira JCF, Martins LASB, Teixeira SFCF. Thermodynamic and economic optimization of a solar-powered Stirling engine for micro-cogeneration purposes. Energy 2016;111:1–17. doi:10.1016/j.energy.2016.05.091.

[18] Moghadam RS, Sayyaadi H, Hosseinzade H. Sizing a solar dish Stirling micro-CHP system for residential application in diverse climatic conditions based on 3E analysis. Energy Convers Manag 2013;75:348–65. doi:10.1016/j.enconman.2013.06.008.

[19] Andraka CE. Dish Stirling advanced latent storage feasibility. Energy Procedia 2014;49:684–93. doi:10.1016/j.egypro.2014.03.074.

[20] Monné C, Bravo Y, Moreno F, Muñoz M. Analysis of a solar dish-Stirling system with hybridization and thermal storage. Int J Energy Environ Eng 2014;5:1–5. doi:10.1007/s40095-014-0080-x.

[21] Kadri Y, Hadj Abdallah H. Performance evaluation of a stand-alone solar dish Stirling system for power generation suitable for off-grid rural electrification. Energy Convers Manag 2016;129:140–56. doi:10.1016/j.enconman.2016.10.024.

[22] Abbas M, Boumeddane B, Said N, Chikouche A. Dish Stirling technology: A 100 MW solar power plant using hydrogen for Algeria. Int J Hydrogen Energy 2011;36:4305–14. doi:10.1016/j.ijhydene.2010.12.114.

[23] Al-Dafaie AMA, Dahdolan ME, Al-Nimr MA. Utilizing the heat rejected from a solar dish Stirling engine in potable water production. Sol Energy 2016;136:317–26. doi:10.1016/j.solener.2016.07.007.

[24] Bumataria RK, Patel NK. Review of Stirling Engines for Pumping Water using Solar Energy as a source of Power. Int J Eng Res Appl 2013;3:864–8.

[25] Li G, Zheng X. Thermal energy storage system integration forms for a sustainable future. Renew Sustain Energy Rev 2016;62:736–57. doi:10.1016/j.rser.2016.04.076.

[26] Yao J, Liu W, Zhang L, Tian B, Dai Y, Huang M. Performance analysis of a residential heating system using borehole heat exchanger coupled with solar assisted PV/T heat pump. Renew Energy 2020.

[27] Esen H, Esen M, Ozsolak O. Modelling and experimental performance analysis of solar-assisted ground source heat pump system. J Exp Theor Artif Intell 2017;29:1–17.

[28] Li H, Bi Y, Qin L, Zang G. Absorption solar-ground source heat pump: Life cycle environmental profile and comparisons. Geothermics 2020;87:101850.

[29] Pavlov GK, Olesen BW. Seasonal solar thermal energy storage through ground heat exchangers. Review of systems and applications. Proceedings, 2011.

[30] Schmidt T, Mangold D, Müller-Steinhagen H. Central solar heating plants with seasonal storage in Germany. Sol Energy 2004;76:165–74.

[31] Sørensen PA, Schmidt T. Design and construction of large scale heat storages for district heating in Denmark. 14th Int. Conf. Energy Storage, 2018, p. 25–8.

[32] Dinçer I, Rosen MA. Thermal Energy Storage. Systems and applications. Wiley; 2011.

[33] Chen Y, Wang J, Lund PD. Sustainability evaluation and sensitivity analysis of district heating systems coupled to geothermal and solar resources. Energy Convers Manag 2020;220:113084.

[34] Panno D, Buscemi A, Beccali M, Chiaruzzi C, Cipriani G, Ciulla G, et al. A solar assisted seasonal borehole thermal energy system for a non-residential building in the Mediterranean area. Sol Energy 2018. doi:10.1016/j.solener.2018.06.014.

[35] Andersson O. BTES for heating and cooling of the Astronomy House in Lund. Therm. Energy Storage Sustain. Energy Consum., Springer; 2007, p. 229–33.

[36] Ferreira AC, Nunes ML, Teixeira JCF, Martins LASB, Teixeira SFCF, Nebra SA. Design of a solar dish Stirling cogeneration system: Application of a multi-objective optimization approach. Appl Therm Eng 2017;123:646–57. doi:https://doi.org/10.1016/j.applthermaleng.2017.05.127.

[37] Buscemi A, Lo Brano V, Chiaruzzi C, Ciulla G, Kalogeri C. A validated energy model of a solar dish-Stirling system considering the cleanliness of mirrors. Appl Energy 2020;260:114378. doi:10.1016/j.apenergy.2019.114378.

[38] Morley SK, Brito T V., Welling DT. Measures of Model Performance Based On the Log Accuracy Ratio. Sp Weather 2018;16:69–88. doi:10.1002/2017SW001669.

[39] Conti P, Testi D, Grassi W. Revised heat transfer modeling of double-U vertical ground-coupled heat exchangers. Appl Therm Eng 2016;106:1257–67. doi:10.1016/j.applthermaleng.2016.06.097.

[40] Incropera FP, DeWitt DP, Bergman TL, Lavine AS. Fundamentals of Heat and Mass Transfer 5th Edition with IHT2.0/FEHT with Users Guides. Wiley; 2001.

[41] Massey BS. Mechanics of fluids. Chapman & Hall; 1989.

[42] Wang X, Zheng M, Zhang W, Zhang S, Yang T. Experimental study of a solar-assisted ground-coupled heat pump system with solar seasonal thermal storage in severe cold areas. Energy Build 2010;42:2104–10.

[43] Klein Sa, Beckman A, Mitchell W, Duffie A. TRNSYS 17-A TRansient SYstems Simulation program. Sol Energy Lab Univ Wisconsin, Madison 2011.

[44] Meteonorm: Meteonorm, Global Meteorological Database. 2015:Handbook part II: theory, version 7.1.7.201517.

[45] D.M. 23 giugno 2016. Incentivazione dell'energia elettrica prodotta da fonti rinnovabili diverse dal fotovoltaico. 2016:8–46.

[46] D. M. 16 Febbraio 2016. Incentivazione della produzione di energia termica da impianti a fonti rinnovabili ed interventi di efficienza energetica di piccole dimensioni 2016:65–71.

[47] Droher JJ, Squier SE. Performance of the Vanguard Solar Dish-Stirling Engine Module. Final report n.d.

[48] Stine W. DR. A Compendium of Solar Dish/Stirling Technology. Sandia Natl Lab 1994:SAND 93-7026.

[49] Mancini T, Heller P, Butler B, Osborn B, Schiel W, Goldberg V, et al. Dish-stirling systems: An overview of development and status. J Sol Energy Eng Trans ASME 2003;125:135–51. doi:10.1115/1.1562634.

[50] Ciulla G, Lo Brano V, D'Amico A, Ciulla G, Lo Brano V, D'Amico A, et al. Modelling relationship among energy demand, climate and office building features: A cluster analysis at European level. Appl Energy 2016;183:1021–34. doi:10.1016/j.apenergy.2016.09.046.

[51] Lo Brano V, Orioli A, Ciulla G, Culotta S. Quality of wind speed fitting distributions for the urban area of Palermo, Italy. Renew Energy 2011;36:1026–39. doi:10.1016/j.renene.2010.09.009.

[52] Kjellsson E, Hellström G, Perers B. Optimization of systems with the combination of ground-source heat pump and solar collectors in dwellings. Energy 2010;35:2667–73.